Materials Today Bio 24 (2024) 100914

Contents lists available at ScienceDirect

Materials Today Bio

journal homepage: www.journals.elsevier.com/materials-today-bio

Heart-on-a-chip systems with tissue-specific functionalities for physiological, pathological, and pharmacological studies

Bingsong Gu [a,b,c,1], Kang Han [a,b,c,1], Hanbo Cao [d,1], Xinxin Huang [a,b,c], Xiao Li [a,b,c,**], Mao Mao [a,b,c], Hui Zhu [a,b,c], Hu Cai [d], Dichen Li [a,b,c], Jiankang He [a,b,c,*]

[a] State Key Laboratory for Manufacturing System Engineering, Xi'an Jiaotong University, Xi' an, 710049, China
[b] National Medical Products Administration (NMPA) Key Laboratory for Research and Evaluation of Additive Manufacturing Medical Devices, Xi'an Jiaotong University, Xi' an, 710049, China
[c] National Innovation Platform (Center) for Industry-Education Integration of Medical Technology, Xi'an Jiaotong University, China
[d] Shaanxi Provincial Institute for Food and Drug Control, Xi' an, 710065, China

ARTICLE INFO

Keywords:
Heart-on-a-chip
Biosensing
Cardiac tissue
Physiological behavior
Pathological modeling
Pharmacological study

ABSTRACT

Recent advances in heart-on-a-chip systems hold great promise to facilitate cardiac physiological, pathological, and pharmacological studies. This review focuses on the development of heart-on-a-chip systems with tissue-specific functionalities. For one thing, the strategies for developing cardiac microtissues on heart-on-a-chip systems that closely mimic the structures and behaviors of the native heart are analyzed, including the imitation of cardiac structural and functional characteristics. For another, the development of techniques for real-time monitoring of biophysical and biochemical signals from cardiac microtissues on heart-on-a-chip systems is introduced, incorporating cardiac electrophysiological signals, contractile activity, and biomarkers. Furthermore, the applications of heart-on-a-chip systems in intelligent cardiac studies are discussed regarding physiological/pathological research and pharmacological assessment. Finally, the future development of heart-on-a-chip toward a higher level of systematization, integration, and maturation is proposed.

1. Introduction

Heart failure is the leading cause of death globally, resulting in about 30 % of all global deaths every year [1–4]. The high mortality of heart failure calls for effective therapeutic strategies and *in vitro* cardiac models. Modern cardiac tissue engineering approaches have made advances in developing highly reliable, and physiologically relevant *in vitro* cardiac models to understand the physiological/pathological mechanisms of the heart and accelerate cardiac-related pharmacological research [5]. To accurately recapitulate cardiac function with the engineered cardiac model, researchers made efforts to organize its cellular and structural cues mimicking the native cardiac tissue. In previous studies, researchers developed various hydrogels or scaffolds with built-in porous or fibrous structures with feature sizes close to the native microenvironment, and cardiac cells were loaded within the ECM for building physiologically relevant cardiac models [6–9]. Recently, 3D bioprinting has emerged as a promising biomanufacturing technology enabling precise control over the spatial and temporal distribution of cells and ECM [10]. With 3D bioprinting, 3D cellularized constructs with geometrical structures of native tissues or organs can be recapitulated, and the architectural mimicry of the native cardiac tissue makes it possible to engineer *in vitro* cardiac models with promising physical and biological relevance [11–13]. In addition, 3D bioprinting can accurately print *in vitro* tissue constructs with single-cell resolution, enabling better resemblance of the cellular microenvironments [14,15]. The high reproducibility and precision of 3D bioprinting techniques gave a further boost to the field of building *in vitro* cardiac models.

In recent years, the *in vitro* cardiac models have been combined with lab-on-a-chip technologies, fueling the growth of heart-on-a-chip systems. Heart-on-a-chip systems are mainly composed of microfluidic chips and on-chip cardiac tissues [16,17]. The microfluidic chip enables the creation of on-demand *in vitro* microenvironments, including the controlled culture medium and gas delivery, to support and regulate the on-chip micro-cardiac tissues in a dynamic manner [18–21]. The

* Corresponding author. State Key Laboratory for Manufacturing System Engineering, Xi'an Jiaotong University, Xi' an, 710049, China.
** Corresponding author. State Key Laboratory for Manufacturing System Engineering, Xi'an Jiaotong University, Xi' an, 710049, China.
E-mail addresses: xiao.li@xjtu.edu.cn (X. Li), jiankanghe@mail.xjtu.edu.cn (J. He).
[1] These authors contributed equally to this work.

https://doi.org/10.1016/j.mtbio.2023.100914
Received 5 October 2023; Received in revised form 8 December 2023; Accepted 12 December 2023
Available online 20 December 2023

on-demand-culture mode provided by the heart-on-a-chip systems allows for the accurate reproduction of cardiac development and disease progression processes *in vitro* [22–25]. Furthermore, significant efforts have been made to integrate various biosensors into the heart-on-a-chip systems for online monitoring of the physiological, pathological, and pharmacological responses in the on-chip cardiac tissues [26,27]. The real-time monitoring manner is promising for precisely collecting information about the incidents happening in the on-chip cardiac tissues at cellular levels, such as the mechanical, electrical, and biochemical behaviors [28–30].

This article reviews the state-of-the-art research in advanced heart-on-a-chip systems that grant tissue-specific functionalities for physiological, pathological, and pharmacological studies. We sum up the current design and capabilities of engineered 3D cardiac constructs recapitulating tissue-specific structures and stimuli on heart-on-a-chip systems. We examine the techniques to integrate sensing components into heart-on-a-chip systems and introduce the interpretation of tissue-specific functionalities with heart-on-a-chip systems from different aspects. Furthermore, we discuss the typical applications of heart-on-a-chip systems in biomedical fields, addressing cardiac physiological, pathological, and pharmacological studies. Finally, we conclude this review with future perspectives for developing more systemized, integrated, and matured heart-on-a-chip systems (Fig. 1).

2. Replicating cardiac constructs with tissue-specific functionalities on the heart-on-a-chip systems

2.1. Requirements for replicating cardiac constructs on the heart-on-a-chip systems

To acquire accurate information in cardiac studies, the cardiac constructs in heart-on-a-chip systems are expected to closely mimic the key characteristics of the native heart, including the structural composition and stimulating properties [22–25]. From the structural composition point of view, the on-chip cardiac constructs need to consist of cardiomyocytes featuring elongated morphology and spatially arranged in specific orientations, which is essential to the restoration of cardiac functions [31,32]. Additionally, the cardiac construct should contain rich and complex vascular vessels to effectively deliver oxygen and nutrients throughout the entire cardiac construct, which are indispensable for maintaining its viability [33]. From the stimulating properties point of view, the heart-on-a-chip system is necessary to contain the dynamic culture environment with mechanical and electrical stimuli mimicking the native heart, which are proven to facilitate the recapitulation of heart pump function *in vitro* [34]. Incidentally, apart from the primary structures and stimuli characteristics, the heart-on-a-chip systems may reflect other features of the human heart, including shear stress caused by the blood flows [35], tissue interfaces [15], and chemical composition changes [36], to name a few.

2.2. Replicating cardiac structural characteristics on the heart-on-a-chip systems

Precise recapitulation of the structures in native cardiac tissue is important to promote the maturation and functional expression of the cardiac construct in heart-on-a-chip systems. Here, in the first part, we discuss the strategies for engineering on-chip cardiac constructs with highly aligned morphology, including the use of micropatterns and 3D scaffolds. In the second part, we summarize the methods to generate vascularized cardiac constructs, including the self-assembly of ECs and 3D bioprinting.

Cell alignment. Micro-contact printing has been used to produce

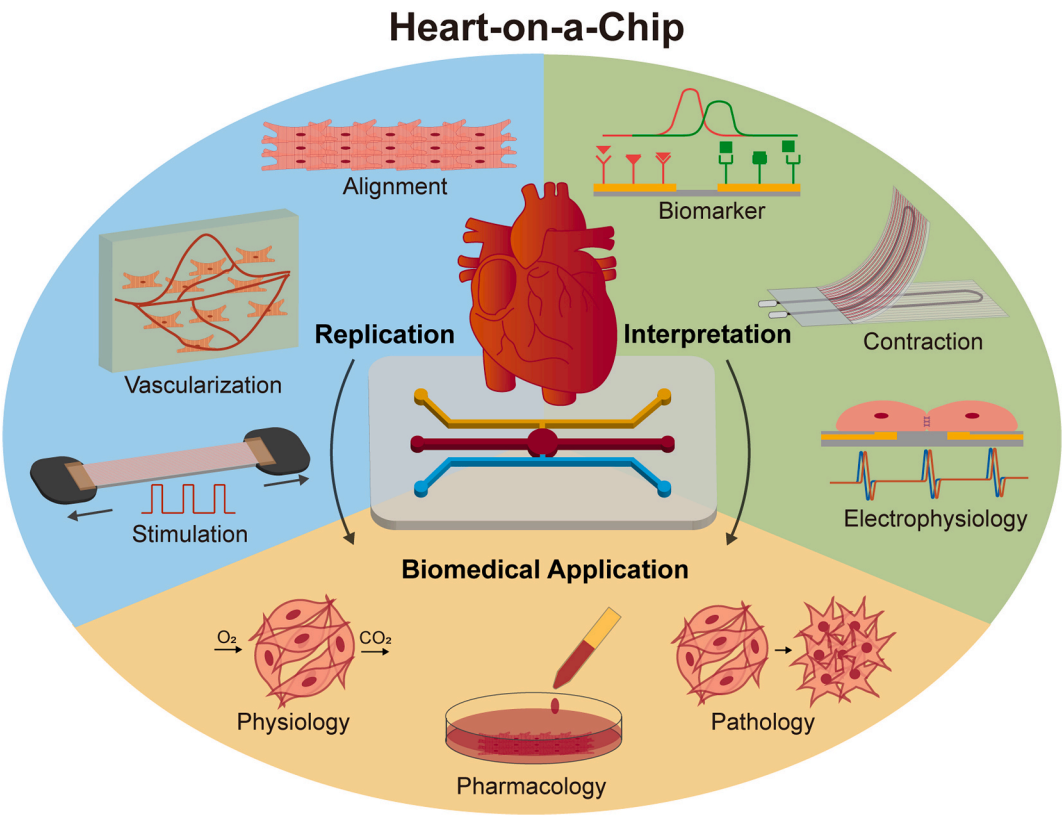

Fig. 1. Advanced heart-on-a-chip systems with replication and interpretation of tissue-specific functionalities for biomedical applications. The schematic indicates that advanced heart-on-a-chip systems should replicate tissue-specific structures and stimuli of the native heart, and interpret tissue-specific functionalities from different aspects. The replication and interpretation of tissue-specific functionalities on advanced heart-on-a-chip systems support typical biomedical applications, including physiological, pathological, and pharmacological studies.

microscale topographical features of extracellular matrix proteins for the guidance of cell alignment [37–39]. For example, Camelliti et al. fabricated a PDMS mold with designed micropatterns based on photolithography, and pressed the mold onto the surface of the culture substrate, forming microchannels that are flushed with a solution containing collagen to deposit tracks for preferential cell attachment. They cultured NRVMs on the substrate with micro-patterned collagen tracks (30 μm in width), and the results showed that the collagen pattern supported the development of cardiac constructs with *in vivo*-like highly-aligned morphology and well-developed sarcomere structure [40]. With a similar contact printing method, Cimetta et al. employed to patterned laminin lane (~100 μm in width) onto poly-acrylamide-based hydrogel, and cardiomyocytes cultured on the patterned hydrogel surfaces were developed into aligned cardiac myofibers with a uniform expression of troponin I [41]. In addition, culture substrate with micro-patterned structures can guide the alignment of cardiac constructs. For example, Lind et al. fabricated PDMS grooves with controllable spacings on the culture substrated by 3D printing. They culture NRVMs on the substrates with grooves at 40, 60, 80, and 100 μm spacing, the results showed that a 60 μm spacing gave rise to the highest cell alignment (Fig. 2A) [42,43].

To better mimic the inherent 3D structure and extracellular

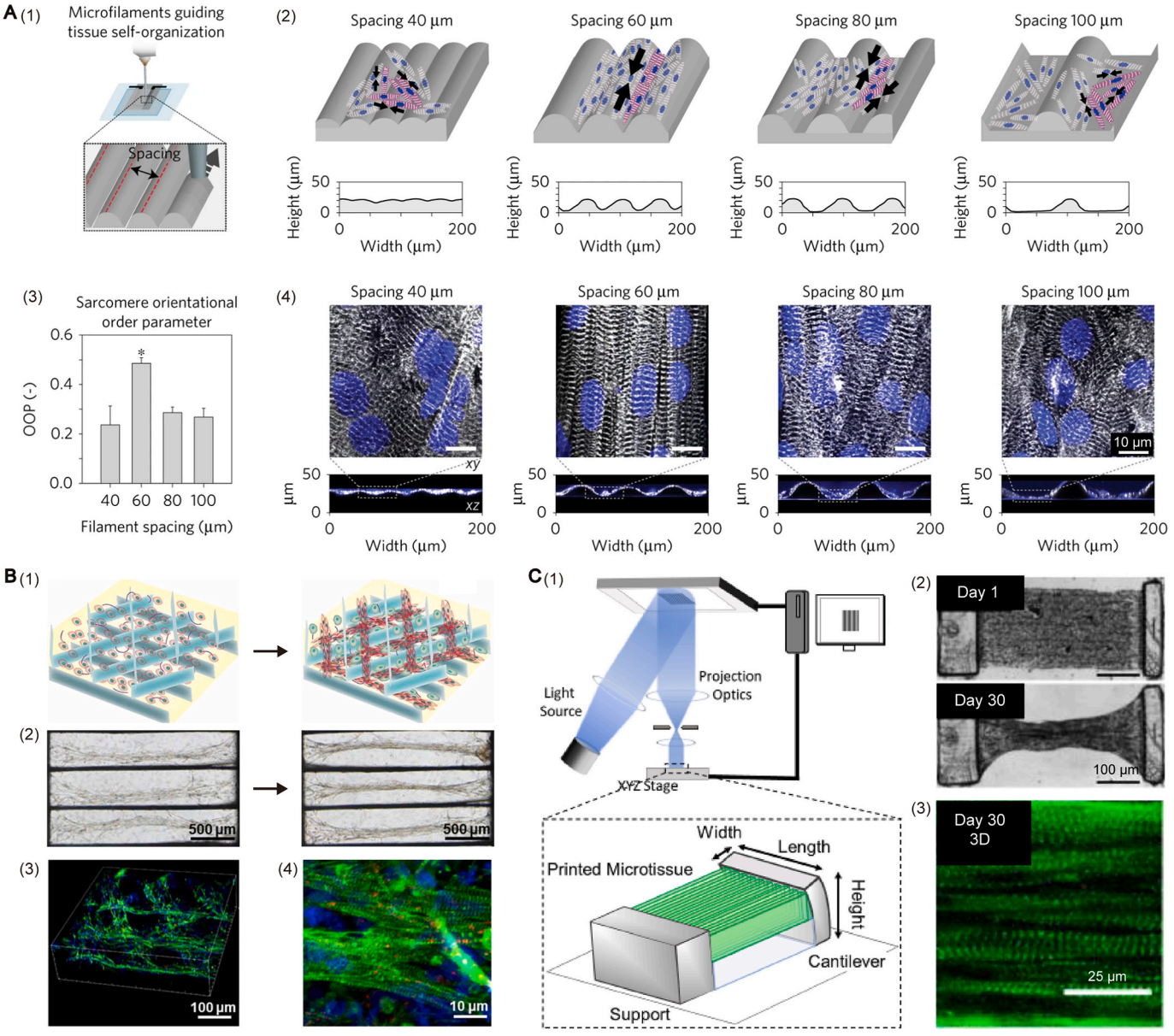

Fig. 2. Strategies for realizing cell alignment in cardiac constructs. A) Recapitulating 2D cardiac cell alignment on 3D-printed PDMS microfilaments. (1) Characterization of the spacing on the PDMS microfilaments. (2) Sketch of microfilaments with filaments printed at 40, 60, 80, and 100 μm spacing guiding self-assembly of engineered cardiac tissue and corresponding stylus profilometer contours of substrates. (3) Sarcomere orientational order parameter of the cardiac construct under 2D culture developed on substrates with 40, 60, 80, and 100 μm filament spacing. (4) Representative confocal images from sarcomere orientational order parameter data. Adapted with permission [42]. Copyright 2017, Springer Nature. B) Recapitulating 3D cardiac cell alignment based on 3D multilayer microfibrous scaffold. (1) Schematic illustrating the seeding and aligning process of cardiomyocyte-laden fibrin hydrogel within the scaffold. (2) Representative optical images of cell alignment inside fibrin. (3–4) Representative immunofluorescence images of 3D cardiac constructs from 3D profile and top view. Adapted with permission [35]. Copyright 2022, IOP Publishing. C) Recapitulating 3D cardiac cell alignment in 3D-printed hydrogel structure. (1) Schematic of the microscale continuous optical printing system. (2) Images of full tissue scaffolds and the compaction the tissue experiences over 30 days. (3) α-actinin stain of day 30 samples Adapted with permission [31]. Copyright 2020, Elsevier.

microenvironment of the native myocardium, aligned 3D cardiac tissues were developed by molding CM-laden hydrogels [8,44–47]. For example, Black et al. fabricated 3D-aligned cardiac constructs by injecting the mixture of CM and fibrin hydrogel in a tubular mold and condensed a cardiac construct composed of aligned cells and ECM fibers inside after a 14-day culture [48]. Bian et al. designed a PDMS mold with in-plane posts regularly arranged according to fiber orientation vectors from a selected epicardial region. After culturing NRVM-laden hydrogel in the mold, 3D cardiac tissue patches (with a large area of 2.5 × 2.5 cm^2, and thickness over 200 μm) with cardiomyocyte alignment that replicated human epicardial fiber orientations were formed [49]. Besides, the mold created pores inside the 3D cardiac tissue patch, and the pores can serve to increase the diffusion of oxygen and nutrients to embedded cells, allowing the viability of the thick tissue [50]. In addition to forming 3D cardiac constructs by casting cell-hydrogel mixture using molds with simple structures, 3D-printed scaffolds with multi-layer complex structures have been applied to produce aligned 3D cardiac tissues. For example, Mao et al. presented a strategy to form aligned tissue constructs by embedding cardiomyocyte/collagen hydrogel into predefined electrohydrodynamically-printed microlattices, and demonstrated the formation of condensed cellular bands aligning along the longitudinal direction of the microlattices [51]. On this basis, Han et al. fabricated 3D multilayer microfibrous scaffolds and pipetted NRVMs-laden fibrin hydrogel within the scaffolds. The 3D scaffold performed a thickness of about 790 μm and varied filament orientation (with an angle of 60° compared with the neighboring bottom layer). After an eight-day culture, a 3D cardiac construct with condensed NRVM bands was formed in the scaffold, and the cardiomyocytes in the constructs demonstrated layer-specific orientations defined by the scaffold (Fig. 2B) [35]. In addition to forming a 3D cardiac construct by seeding CM-laden hydrogel within supporting scaffolds, CM-laden hydrogel can be shaped by optical bioprinting. For example, Liu et al. developed microscale continuous optical printing for rapid structuring of cardiomyocytes encapsulated in a GelMA structure. Thay demonstrated the fabrication of a 3D CM-laden hydrogel construct with initial dimensions of 1.9 × 0.91 × 0.21 mm (length × width × height). After a 30-day culture, the width of the cardiac construct contracted to ~290 μm, and additionally, the encapsulated cardiomyocytes showed elongated morphology and highly aligned arrangement close to the phenotypic of *in vivo* cardiac tissues (Fig. 2C) [31].

Vascularization. The main reason for the necessity of vascularization for the engineered 3D cardiac construct is that oxygen diffusion is limited to a depth of about 100 μm from the tissue surface, and the inner cells of 3D tissues become necrotic due to the lack of oxygen [36,52–54]. It has been demonstrated that the ECs, the main constituent cells of the inner lining of blood vessels, are intrinsically able to engineer microvascular networks in *vitro*, and the network was proved to exhibit enhanced viability and persistence by co-culturing with supporting cells [55]. In recent years, researchers have developed vascularized cardiac constructs *in vitro* by co-culture of cardiomyocytes, ECs, and supporting cells. For example, Tsukamoto et al. cultured hiPSC-CMs with NHCFs and HMVECs to fabricate 3D vascularized cardiac constructs, and microvascular networks are proved to be evenly distributed in the engineered 3D cardiac construct with a 5-day culture (Fig. 3A) [56]. Moreover, Justine et al. established a co-culture system including NRVMs: hASCs: HUVECs at an optimized cell ratio of 1,500,000:37, 500:150,000 cells/cm^2 to engineer a functional cardiac construct with dense vasculature network assembly. The engineered cardiac construct showed statistically identical electrophysiological functionalities to the NRVM-only construct, exhibiting an electrical conduction velocity of about 14 cm/s, APD80 of about 152 ms, and APD30 of about 71 ms [57].

In recent years, vascularized 3D cardiac constructs have been developed based on 3D printing. One strategy is producing a 3D scaffold with vascular-like structures based on 3D printing and then culturing cardiomyocytes onto the scaffold. Specifically, researchers have developed ECs-laden bioinks for 3D bioprinting and demonstrated the printing of a 3D scaffold of microfibers with highly-defined orientation and controllable diameter from 300 to 150 μm. Due to the low viscosity of the bioink, the ECs can gradually migrate towards the peripheries of the microfibers forming confluent vasculars [59,60]. By seeding cardiomyocytes to the 3D scaffold with microvascular structures, cardiomyocytes can gradually adhere to the microvascular structures. For example, Zhang et al. printed HUVECs-laden microfibrous scaffolds (fiber diameter of ~150 μm), and demonstrated the HUVECs inside the fibers gradually migrate to surround the microfibers forming confluent microvasculars over a 15-day culture. Neonatal rat cardiomyocyte suspension was then pipetted to the as-formed vascularized scaffold, and the cardiomyocytes were demonstrated to attach and align on the outside of the microvascular, together assuming the configuration of an *in vitro* endothelialized myocardial tissue resembling the structure of a native myocardium containing blood vessels (Fig. 3B) [9]. Another strategy is building a 3D cardiac construct at first and then creating the embedded channels as perfusable vasculars using 3D printing. For example, Mark et al. prepared a 3D cardiac construct with the shape of a normal human heart by casting hiPSC-CMs derived organ building blocks with a 3D mold. Then the sacrificial ink was printed inside the cardiac construct, and the printing trajectory was designed according to the left anterior descending coronary artery of the human heart. Finally, the artery-like structure of sacrificial ink was removed by 37 °C incubation, leaving behind a 3D network of hollow channels as the perfusable vascular inside the 3D cardiac construct (Fig. 3C) [58]. Furthermore, multi-nozzle 3D printing was applied to build cardiac construct together with vascular networks. For example, Noor et al. demonstrated 3D printing of iPSC-CM-laden omentum hydrogel (OM + CM) and EC-laden gelatin (sacrificial layer + EC) using separate printing heads, and they performed the construction of a thick 3D cardiac construct (with a thickness of about 2 mm) embedded with gelatin channel containing blood vessel-forming ECs. After incubation at 37 °C, the ECs moved to the boundary of the omentum hydrogel and the gelating was washed out, exhibiting open cell lumens with a diameter of about 300 μm in the cardiac construct, assuming the formation of vascular channels inside the 3D cardiac construct (Fig. 3D) [11].

2.3. Replicating cardiac stimulating characteristics on the heart-on-a-chip systems

The development and function of the native heart involve mechanical and electrical stimuli. These stimuli help to organize the overall structure of the tissue, encourage cell elongation, and increase cell length-to-width ratio, all of which affect the function of cardiac tissues including cellular maturation phenotypes and contractile activities [61–63]. In this section, we summarized the effect of mechanical and electrical stimulation applied to on-chip cardiac constructs in passive or active manners to achieve greater cardiomyocyte maturation and functional development.

Mechanical stimulation. Mechanical stimulation has been frequently applied to drive the maturation of *in vitro* cardiac constructs, and according to the mechanical loading mode we characterized the mechanical stimulation into a passive and active load. Specifically, the mechanical property of the structure (such as the stiffness) that interacts with the cardiac construct in a static mode was considered as the passive load. For example, it has been shown that the stiffness of the extracellular matrix can alter the cellular shape, sarcomere organization, and contraction behavior of the adherent cardiomyocytes [64–67]. Bhana et al. prepared collagen-coated polyacrylamide hydrogel with different stiffness (with Young's moduli of 3, 22, 50, and 144 kPa) to characterize the influence of substrate stiffness on the functional development of neonatal rat cardiomyocytes, and the results indicated that a medium hydrogel stiffness (~50 kPa) was optimal for the functional development of cardiac cells, including the matured sarcomere, high contractility, and reasonable electrical excitation threshold [68]. Further, a passive mechanical load was proved to alter the development process of

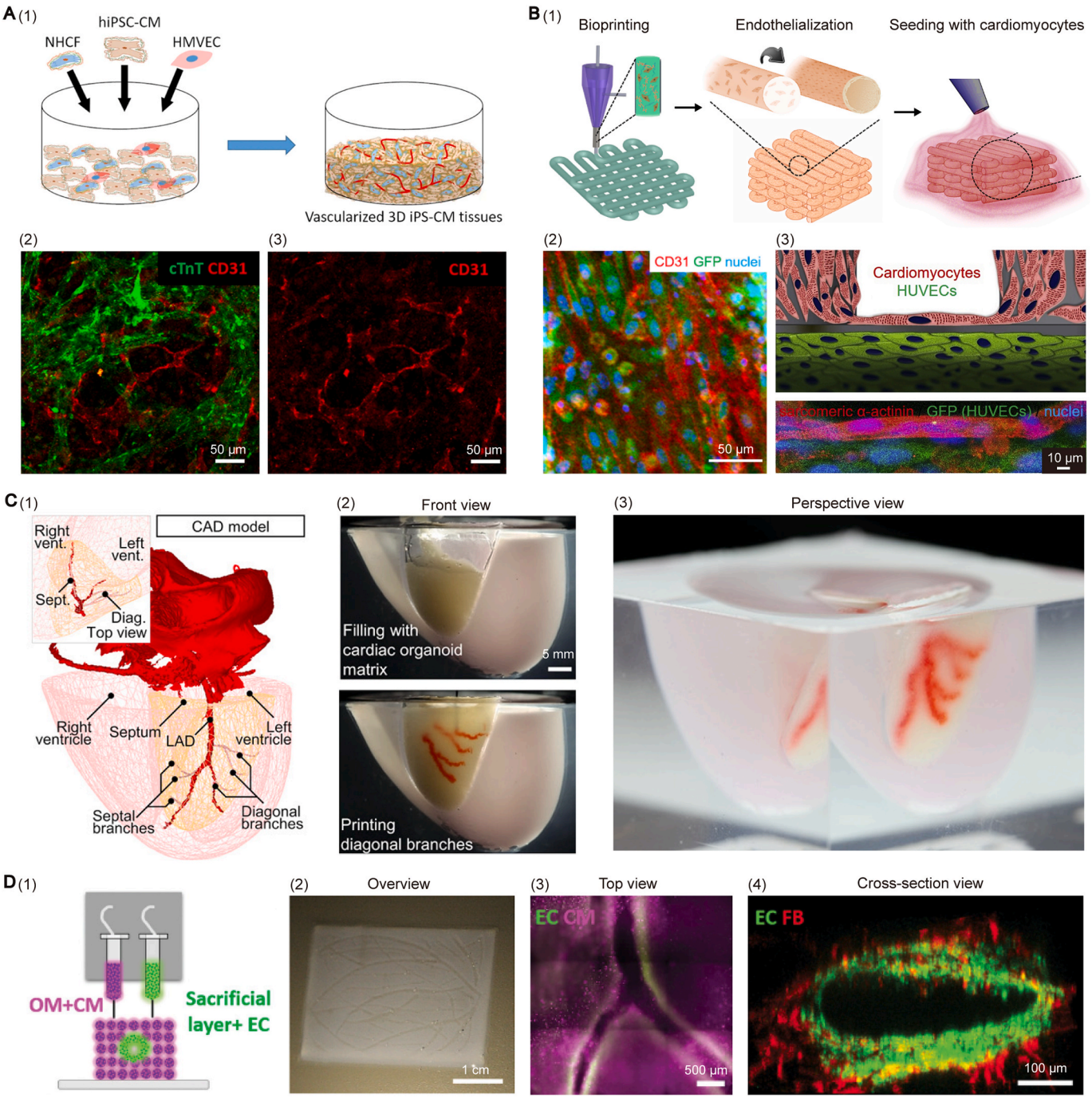

Fig. 3. Strategies for realizing vascularization in cardiac constructs. A) Vascularized cardiac construct produced by co-culture of multiple types of cells. (1) Schematic showing the fabrication of the vascularized 3D cardiac construct by co-culturing of hiPSC-CM, NHCFs, and HMVEC. (2) The merged image of cTnT and CD31 (3) The CD31 image. Adapted with permission [56]. Copyright 2020, Springer Nature. B). Vascularized 3D cardiac constructs produced by printing endothelialized scaffold. (1) Schematics showing the procedure of fabricating the vascularized 3D cardiac constructs with three steps: 3D bioprinting of ECs-laden fibrous scaffold, ECs migration forming endothelialized structure in the scaffold, and seeding cardiomyocytes onto the endothelialized scaffold. (2) Confocal fluorescence micrograph showing the expression of CD31, GFP, and nuclei in a single fiber. (3) Schematic and high-resolution confocal fluorescence micrograph showing an endothelialized myocardial tissue formed by seeding neonatal rat cardiomyocytes onto the bioprinted endothelialized microfibrous scaffold after endothelialization. Adapted with permission [9]. Copyright 2016, Elsevier. C) Vascularized 3D cardiac constructs produced by printing sacrificial structures. (1) The 3D CAD model of a normal human heart. (2–3) The front and perspective view of the printed diagonal branches within the cardiac organoid matrix. Adapted with permission [58]. Copyright 2019, The authors. D) Vascularized 3D cardiac constructs produced by multi-nozzle 3D printing. (1) A side view of the printing concept and the distinct cellular bioinks. (2) A printed thick cardiac construct with embedded vascular-like channels. (3) A fluorescent image indicating blood vessels composed of ECs is seen in between the cardiac construct. (4) Cross-sections of a single lumen, showing the interactions of GFP-expressing ECs. Adapted with permission [11]. Copyright 2019, The Authors.

the 3D cardiac constructs. For example, Bliley et al. bounded 3D cardiac bundles to elastic PDMS strips with two sets of bending stiffness (denoted by 1 × and 8 ×), and the stripes imposed low (1 ×) and high (8 ×) force onto the cardiac bundles. The results indicated that the strip with higher mechanical loading (8 ×) enhanced the function of the engineered cardiac construct with improved cell alignment, cardiac contractility, and electrical conduction velocity. In addition, the genes associated with different aspects of the contractile apparatus were

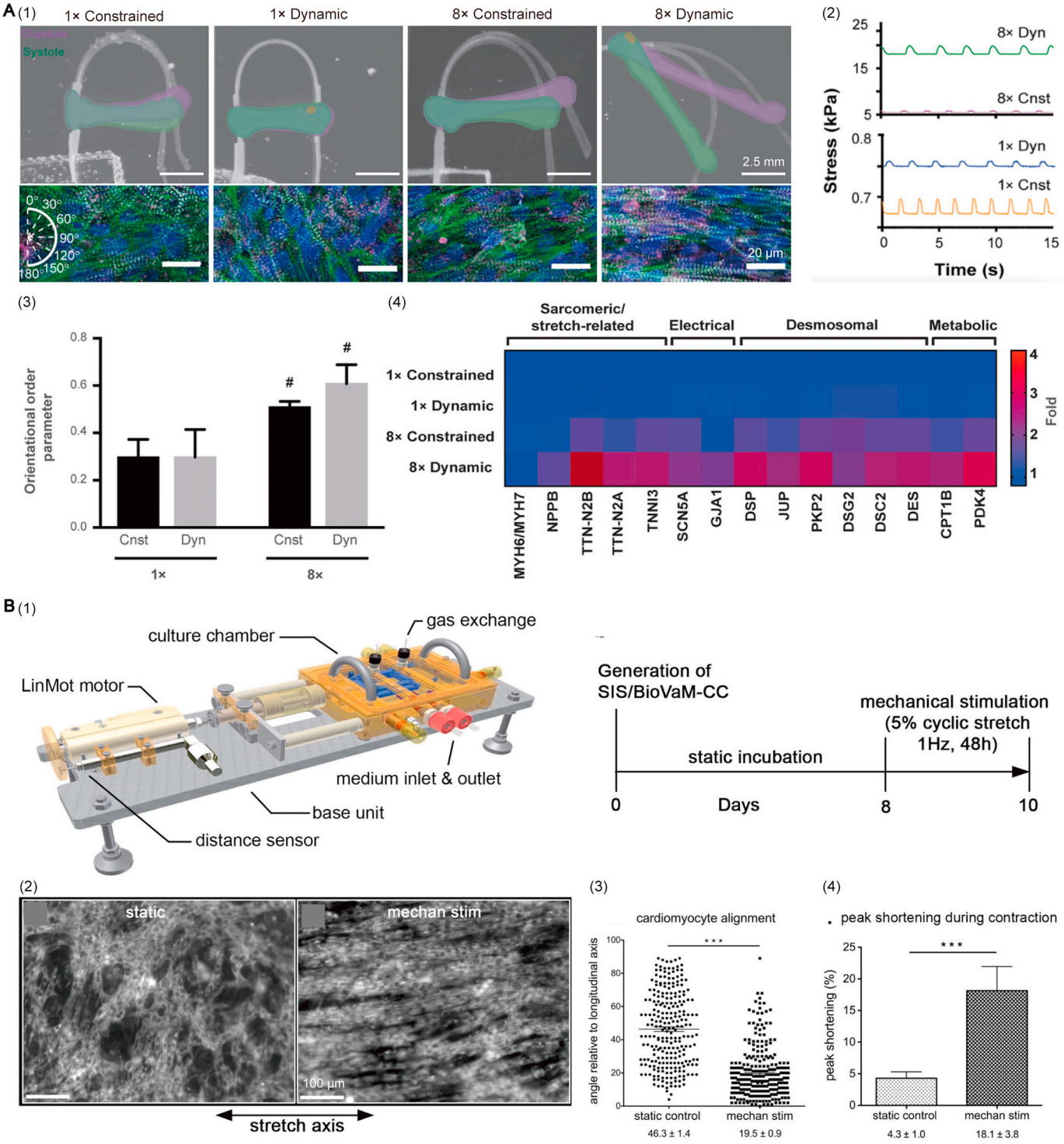

Fig. 4. Promote functional development of cardiac constructs by mechanical stimulation. A) PDMS strips with different bending stiffness (1 × and 8 ×) are used to mechanically load engineered cardiac constructs. (1) Macroscopic tissue contractions overlaid with tissue in systole and tissue in diastole and corresponding fluorescent images of tissue surfaces under each loading condition. (2) Cardiomyocyte stress during contraction and relaxation. (3) Tissue diastolic stress/tensile stress. (4) Heatmap showing log scale geometrical mean of gene expression relative to the 1 × constrained loading condition. Adapted with permission [69]. Copyright 2021, The Authors. B) Promote the maturation of cardiac constructs by the active uniaxial cyclic stretch. (1) Schematic shows the bioreactor design and outline of the stimulation protocol. (2) TMRM + staining of cardiac construct cultured under static and mechanically stimulated conditions. (3) Quantification of cell alignment. (4) Quantification of maximal peak shortening during contractions. Adapted with permission [71] Copyright 2016, Elsevier.

observably up-regulated under the 8 × mechanical loading (Fig. 4A) [69]. The mechanical stimulation that interacts with the cardiac construct in a dynamic mode (such as cyclic shear stress or oriented stretch) was considered as the active load. For example, Jackman et al. fabricated 3D cardiac bundles using NRVMs or hiPSC-CMs and cultured the cardio bundles on a rocking platform. The results indicated that the NRVM-cardio bundles showed an average contractile force per cross-sectional area of 59.7 mN/mm^2 and a conduction velocity of action potentials of 52.5 cm/s, which was similar to or identical to adult rat myocardium. In addition, the human cardiobundles cultured under active mechanical stimulation showed an average contractile force of 23.2 mN/mm^2 and a conduction velocity of 25.8 cm/s, closing to the functioning parameters of the adult human myocardium [70]. Lux et al. developed cultured a large-scale (2.5 × 4.5 cm) 3D cardiac construct and applied 5 % uniaxial cyclic stretch (2.2 mm) at 1 Hz for 48 h starting at day 8 of cultivation, and the results showed a uniaxial contraction of aligned cardiomyocytes (with an average angle about 20°) resulted in higher peak shortening of stimulated constructs compared to static controls (Fig. 4B) [71].

Electrical stimulation. The native heart is composed of a group of electroactive cardiomyocytes and electrically conductive fibers, the conductive-fiber network improves the electrical communication between adjacent cardiomyocytes [72]. Mimicking such electrically conductive features, electrically conductive materials as passive cues were introduced in fibrous scaffolds for generating 3D cardiac constructs [73]. For example, Wang et al. prepared PLA/PANI scaffolds with different electrical conductivity and cultured neonatal rat primary cardiomyocytes cultured on those conductive scaffolds. The results showed

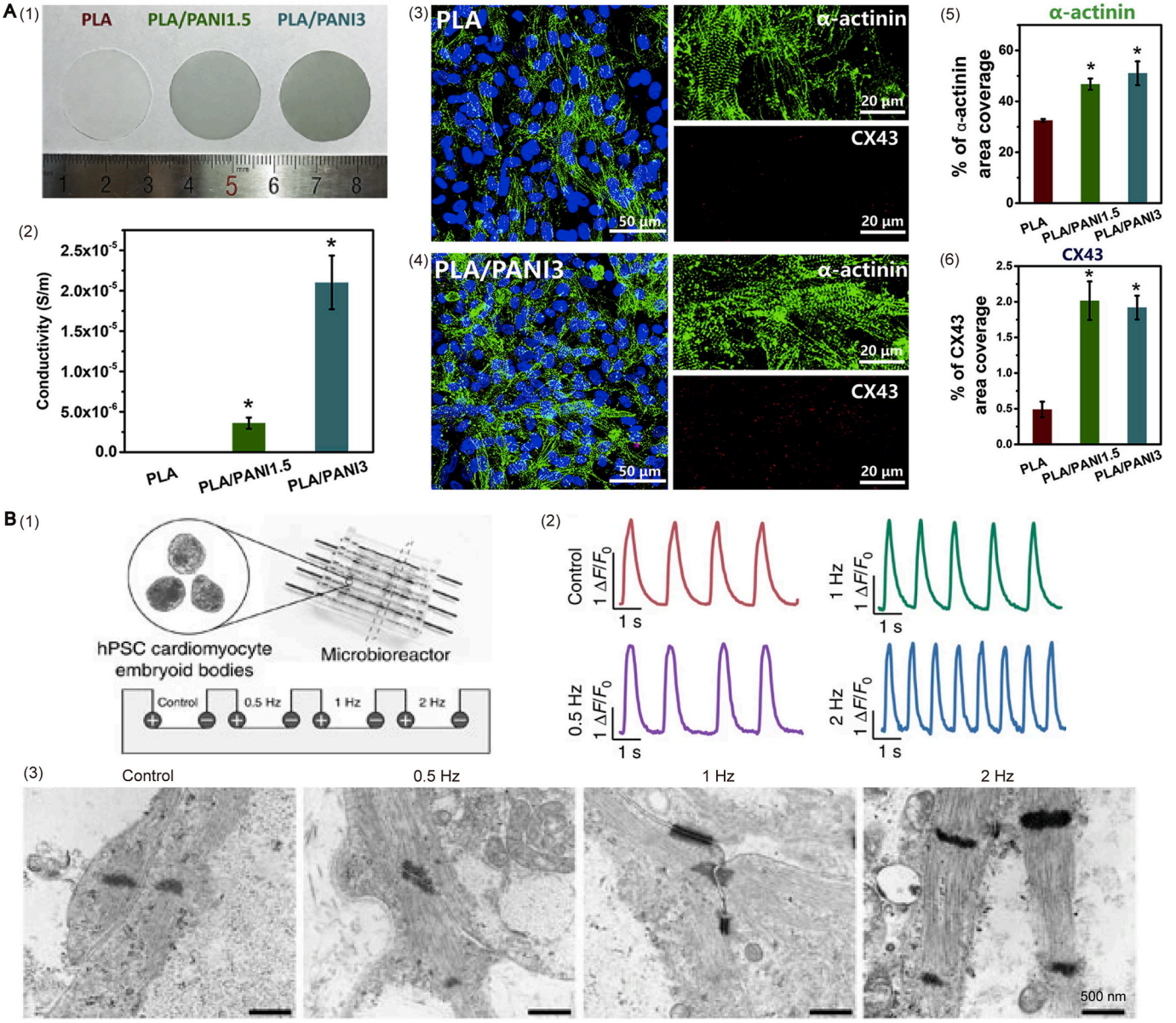

Fig. 5. Promote functional development of cardiac constructs by electrical stimuli. A) Promote the maturation of cardiac constructs using electrically conductive scaffolds. (1) Optical images of PLA/PANI nanofibrous sheets with different PANI concentrations including 0 wt%, 1.5 wt%, and 3 wt%. (2) The electrical conductivity of PLA/PANI samples. (3–4) Representative fluorescence images of CMs immunostained for sarcomeric α-actinin (green) and CX43 (red) on PLA and PLA/PANI (3 wt%). (5–6) The area fraction of α-actinin and CX43. Adapted with permission [74]. Copyright 2021, Elsevier. B) Promote the maturation of cardiac constructs by active electrical stimulation. (1) Schematic of microbioreactor set-up. (2) Calcium fluorescence traces for an entire beating area over time. (3) Transmission electron microscopy image illustrating the thickness of sarcomere in cardiomyocytes under different stimulation frequencies. Adapted with permission [76]. Copyright 2016. Springer Nature. (For interpretation of the references to color in this figure legend, the reader is referred to the Web version of this article.)

that the higher electrical conductivity induced more expression of sarcomeric α-actinin and connexin 43 (CX43), indicating enhanced cardiac maturation (Fig. 5A) [74]. In addition, electrically conductive materials were combined with hydrogel to provide a 3D electrically conductive environment to promote the maturation of cardiac constructs. For example, Roshanbinfar et al. cultured a 3D cardiac construct based on biohybrid conductive hydrogels composed of alginate, collagen, and PEDOT: PSS. The results indicated that the sarcomeric length of cardiomyocytes in the construct was about 1.9 μm and cardiac contractility reached 200 beats per minute, suggesting the formation of mature cardiac tissue by using the conductive hydrogel [75].

The native myocardium is composed of specialized cells called pacemaker cells that generate electrical pulses spontaneously for regulating and controlling the synchronized contraction of cardiac tissue [61]. Mimicking this, external electrical stimulation has been introduced to the *in vitro* culture of cardiac constructs. For example, George et al. cultured 3D embryoid bodies composed of human stem cell-derived cardiomyocytes under external electrical stimulation with different frequencies (5 V/cm at 0.5, 1, and 2 Hz), and the results showed that cardiac constructs cultured under 2 Hz stimulus exhibited thick sarcomere (approximately 600 nm) and enhanced calcium cycling, indicating the electrical conditioning promotes cardiomyocyte maturation in 3D culture (Fig. 5B) [76].

3. Interpreting tissue-specific functionalities from different aspects of the heart-on-a-chip systems

3.1. Requirements for interpreting cardiac information on the heart-on-a-chip systems

Based on accurately representing the essential structures and functions of the human heart, heart-on-a-chip systems further demand intelligent techniques to support the interpretation of meaningful information from the *in vitro* cardiac models. Traditionally, numerous biological assays provided basic information on the on-chip cardiac tissue, such as cell confluence, cell viability, cell proliferation, and protein expression [77,78]. As the specific function of cardiac tissue, the spontaneous contractile behavior and underlying inter- and sub-cellular electrophysiological activity are essential for understanding cardiac function. Specifically, the electrical activation of cardiomyocytes is generated from the cross-membrane ion flows (such as the Na^+, K^+, and Ca^{2+}) that can be recognized as the action potentials (also known as, the transmembrane current). Successively, the action potential activates the opening of the Ca^{2+} channel on the cardiomyocyte membrane, and the inward-flowed Ca^{2+} induces the release of Ca^{2+} stored in the sarcoplasmic reticulum. The transiently rising of Ca^{2+} concentration causes the sliding between sarcomere protein filaments, which causes the whole cardiomyocyte to exhibit contraction. After a contraction, the cell membrane actively transports Ca^{2+} to the outside of the cell while the cardiomyocyte begins to diastole. Moreover, the electrophysiological activity can be conducted through structural connections (such as the gap junction protein, cx43) from cell to cell transiently, inducing the synchronized contraction of the whole heart (Fig. 6) [79–84].

Normally, *in vitro* cardiac models are analyzed with optical microscopy to observe the morphology of cells/tissues, the frequency and amplitude of the spontaneous contractile behaviors can be registered through microscopic imaging, but the mechanical forces generated by the contraction might not be accurately quantified. Moreover, with the addition of fluorescent indicators, the electrophysiological activity can be reflected by optical fluorescent microscopy, such as ultra-high-resolution microscopes that break through the diffraction limit to observe fine fluorescent incidents with resolution smaller than 200 nm and multi-photon imaging systems for deep fluorescent imaging of thick tissues. A typical application of observing cardiac electrophysiological activity by optical observation is calcium transient fluorescent imaging. For example, *in vitro* cardiomyocytes or cardiac tissues were immersed with the Ca^{2+} dye (e.g., Fluo-3, Fluo-4, Rhod-2) that can bind with the Ca^{2+} moving across the cellular membranes, and the fluorescence intensity of the indicator increases significantly after binding with the Ca^{2+} [85–87]. Based on this principle, the flow of Ca^{2+} can be recognized using optical fluorescent image techniques. However, the intervention of the fluorescent dyes can interfere with the normal functioning of cardiomyocytes, and the fluorescence intensity of the dye decays gradually after staining which hinders prolonged observing. In addition to the optical fluorescent observation, patch clamp is another commonly used technique for *in vitro* cardiac electrophysiological study. The patch clamp technique applies a glass microelectrode with a tip diameter of 1.5–3 μm to contact the surface of the cell membrane, and a small area of the cell membrane under the tip of the electrode is electrically separated from its surroundings, and the ionic currents through the ion channels on this patch are monitored [88,89]. Among the existing electrophysiological recording methods, patch-clamp is a “gold standard” for obtaining high-quality electrophysiological signals, but it is limited to single-cell measurement and cannot readily access the cellular signals within 3D cardiac tissues. In addition, its rigid syringe electrode structure can cause damage to the cell making it difficult to monitor active tissues for a long time.

As we discussed, the cardiac-specific functionalities are mainly represented by contractile behaviors and electrophysiological activities. Conventional optical observation and patch clamp recording methods offered a faithful interpretation of these cardiac-specific functionalities but each has its limitations. Besides, these methods call for specialized

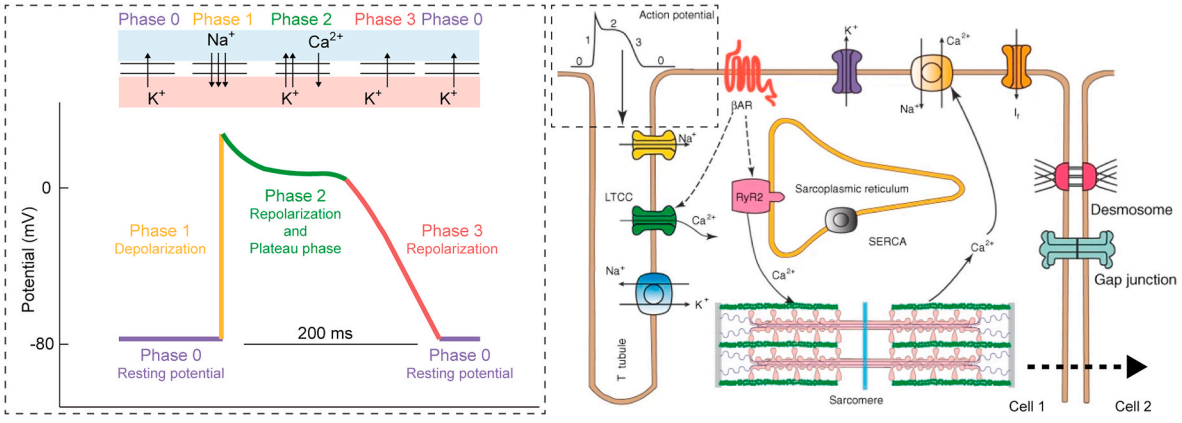

Fig. 6. Schematics showing physiological mechanisms related to cardiomyocyte contraction. The generation process of a normal action potential and the following cardiomyocyte contraction, including ion dynamics, sliding of sarcomere filaments, and intercellular communication. Adapted with permission [82]. Copyright 2022, Springer Nature.

equipment and operators. To effectively interpret these tissue-specific functionalities on a heart-on-a-chip system, there are two major requirements: ensuring the integrity of the on-chip cardiac tissue during the observing process; achieving prolonged monitoring to realize real-time analysis of cardiac information throughout the whole life cycle of the *in vitro* cardiac model. Moreover, the heart-on-a-chip system needs to accurately reveal the condition of the cardiac model. To meet these requirements, an effective method is introducing specific biocompatible microsensors into the heart-on-a-chip system to vividly convert different types of physiological information into computable physical quantities. In this section, we discuss sensing techniques for interpreting tissue-specific functionalities in heart-on-a-chip systems, including cardiac electrophysiological signal recording and contractile activity measurement. In addition, we summarize the recently reported methods of realizing online sensing of cardiac-specific biomarkers in heart-on-a-chip systems.

3.2. Interpreting cardiac electrophysiological signals on the heart-on-a-chip systems

Cardiac tissues function under the orchestration of electrophysiological signals, and the precise characterization of the cardiac electrophysiological signals in addition to cardiac contractile monitoring is important to a deeper understanding of cardiac physiological and pathological mechanisms. Based on the development of microsensors, microelectrode array devices have been integrated into heart-on-a-chip systems to realize online monitoring of the electrophysiology of cardiac constructs. According to the type of the recorded electrophysiological signals, we summarized microelectrode array devices including extracellular and intracellular recording devices.

Extracellular recording. For extracellular recording, electrical coupling between cardiomyocytes and micro-scale planar electrodes is established by adhering cardiomyocytes onto the microelectrodes, and extracellular action potential changes because of the ionic flow through the cell membranes. The parameters (e.g., amplitude, duration, and firing rate) of extracellular potential, can be analyzed by the MEA recordings, and the change in potential subsequently propagates along the adjacent cardiomyocytes can also be analyzed. The basic application of MEAs on a heart-on-a-chip model is detecting electrophysiological signals from the cardiac syncytial layer on a planar substrate (Fig. 7A). For example, Liang et al. produced an on-chip electrophysiological sensor in the form of gold microelectrodes, on which a confluent monolayer of spontaneously contracting HL-1 cardiac cells resided. Electrophysiological signals from different sites were recorded synchronously, which have a synchronized beating rate of 5 Hz. In addition, the propagation of cardiac action potentials over the cardiac construct was visualized as an isochronal map of time latencies, indicating a propagation velocity of about 10 mm/s (Fig. 7B) [90]. Nevertheless, the cardiac syncytial layer lacks revealing the cell-cell communication in a functional cardiac tissue, and 3D cardiac constructs were developed to solve this problem, which provided venues to understand the coordination and function of systems functional cardiac tissue. To provide a multisite and simultaneous investigation of cardiac electrophysiological signals on 3D cardiac constructs. For example, Kalmykov et al. produced 3D self-rolled biosensor arrays consisting of microelectrodes on a soft thin film, and they rolled the device around a prepared human cardiac spheroid. With this setup, multi-channel electrophysiological signals acquired from the 3D surface of the cardiac construct displayed evident time latencies between signals from different sites recorded from the spheroid, and the conduction velocity was calculated as the gradient from the extrapolated time latency isochronal map averaging at 12.45 ± 1.88 cm/s (Fig. 7C) [91]. Gu et al. integrated Pt microelectrodes in a 3D cardiac construct with highly-aligned morphology and performed *in situ* 3-channel extracellular recording along the cardiac construct. They demonstrated that the amplitudes of the recorded extracellular signals in the cardiac construct were between 10 and 155 μV, and the conduction velocities of the extracellular signal along the cardiac construct were in the range of 22.09 ± 2.02 to 26.34 ± 1.93 cm/s during 50-h culture (Fig. 7D) [92]. Moreover, to interpret the electrophysiological signals inside 3D cardiac constructs, mesh electronics with microelectrodes was applied to deeply integrate with the cardiac constructs. For example, Dai et al. produced an ultrathin 2D free-standing mesh electronic consisting of 64 addressable electrodes with subcellular dimensions. They folded the device into a 3D-multilayered feature and embedded the device inside 3D cardiac tissues, which enabled simultaneous multisite stimulation and mapping of the real-time dynamics of extracellular action potentials in cardiac models [93]. Li et al. reported stretchable mesh nanoelectronics and uniformly integrated the device inside 3D cardiac organoids. Notably, the integration process was driven by the cell−cell attraction forces during the 3D self-condensation and organization of cells. With this intimate integration, electrophysiological patterns during organogenesis were studied and the recorded electrophysiological data suggested that the functional maturation of a cardiac organoid is marked by the synchronization of its electrophysiological activities (Fig. 7E) [94].

Intracellular recording. Micro/nanoscale features of recording electrodes can help access intracellular signals from cardiomyocytes. Conventional planar microelectrodes suffer from a low signal-to-noise ratio (SNR) due to the poor coupling between cells and electrodes, which leads to a small sealing impedance and small signal amplitude [95]. To improve the signal quality and closely interrogate the cardiac ion channels, nano-scale features (e.g., carbon nanotubes, platinum black, ZnO nanowires) were introduced to the surface of microelectrodes to enhance the coupling between the cell membrane and electrode (Fig. 8A) [96,97]. For example, Hu et al. prepared a unique nano-branched microelectrode array by combining ZnO nano-branches onto microelectrodes and sputtering onto the surface. The 3D structure of nano-branches enables the electrode to form tight coupling with cardiomyocytes to achieve low-voltage cell electroporation and high-quality intracellular recording. The recorded intracellular action potentials of cardiomyocytes exhibited significant enhancement in amplitude (~5 mV), SNR (~67.47 dB), recording duration (up to 105 min), and recording yield (69.5 ± 17.8 %) (Fig. 8B) [98]. Although the application of nano-scale cues can improve the quality of recorded electrophysiological signals, the improvement was still limited because the shape of the cues cannot be controlled accurately. To further improve the signal quality, 3D nanostructured intracellular electrodes have been developed to deeply interface with cell membranes [99]. In addition, in-cell recording of action potentials from cardiomyocytes with high quality can be realized by employing membrane-poration techniques including electroporation, optoporation, and membrane fusion. For example, Xie et al. applied Pt nanopillar electrodes (1.5 μm in length and 150 nm in diameter) to detect the action potential of HL-1 cardiac cells, they demonstrated consistent in-cell recording and the recorded signal amplitude reached 11.8 mV (Fig. 8C) [100]. Further, Lin et al. developed nanoelectrodes in shape of nanotube and demonstrated that cell membrane not only wraps around the vertical tubes but also protrudes deep into the hollow center. The wrapping and protruding induced a tight membrane/electrode interface that largely increased the seal resistance, and the amplitude of the recorded signals reached 15 mV after electroporation (Fig. 8D) [101]. Desbiolles et al. fabricated volcano-shaped microelectrodes that showed ability to fuse with the cell membrane, which provided passive intracellular access to cardiomyocytes and continuous in-cell recording was realized reached amplitude as high as 20 mV (Fig. 8E) [102]. In more recent research, Cui group reported vertically-aligned nanocrown electrodes that demonstrated a hollow platinum crown 180–200 nm deep for the 3 μm-tall structure and the shape can induce the cell membrane to wrap around the outer surface while promoting cell adhesion to the inner core at the same time. Remarkably, they demonstrated electrophysiological recording from cardiomyocytes with signal amplitude up to ~63 mV, and the recorded waveform have only overall deviation ~1 % compared

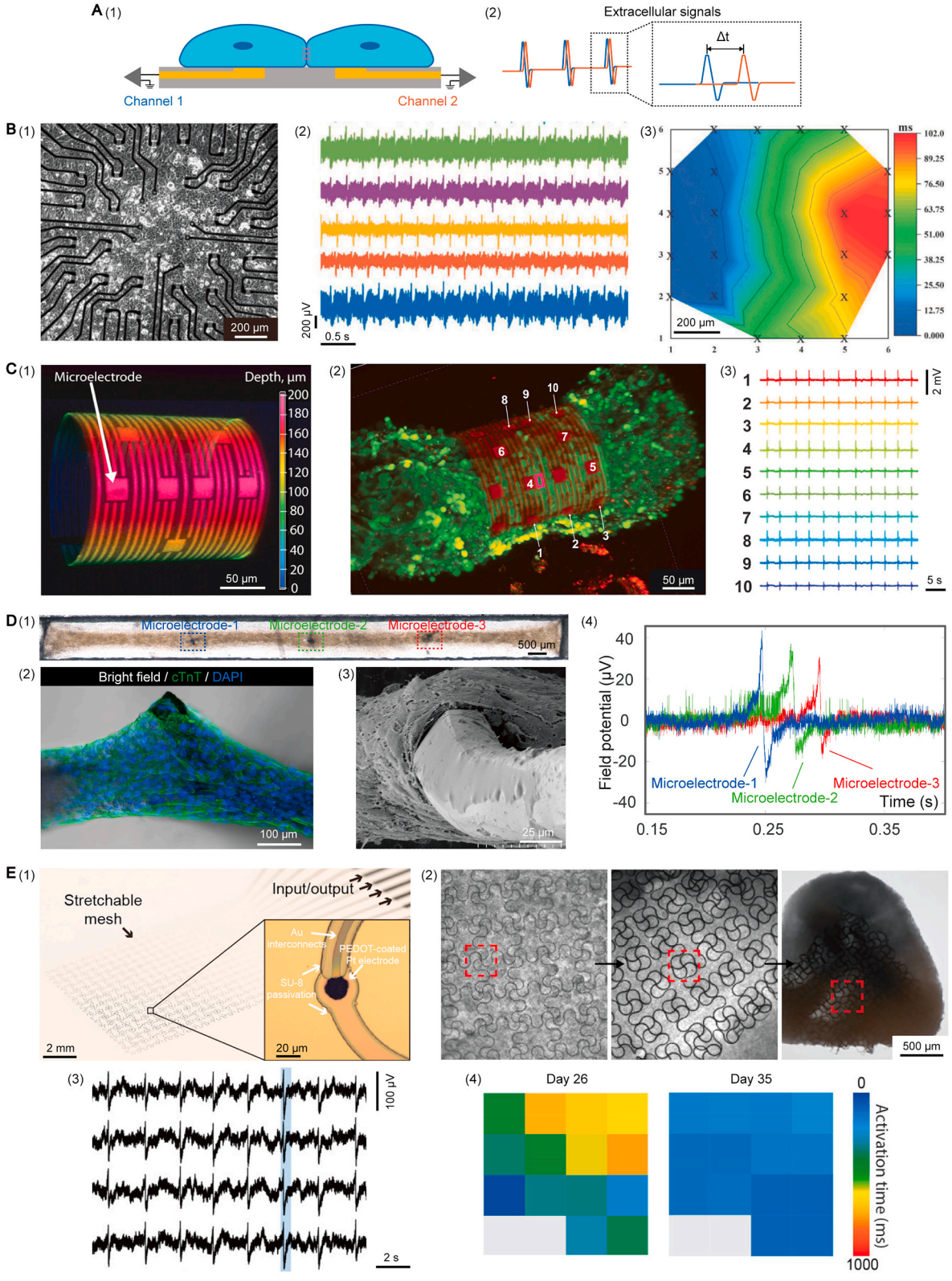

(caption on next page)

Fig. 7. Extracellular electrophysiological recording. A) Schematics depict (1) the spatial relationships between a cardiomyocyte and a planar microelectrode for extracellular electrophysiological recording, and (2) typical form of extracellular signals. B) Planar extracellular recording device. (1) Optical image of HL-1 cells on the surface of the device. (2) Representative action potential spikes. (3) The contour map of activation time based on the action potential propagation. Adapted with permission [90]. Copyright 2018, WILEY-VCH. C) Flexible extracellular recording wrapped on a 3D cardiac organoid, and multi-site signals from the surface of the 3D cardiac organoid. (1) 3D confocal microscopy image of 3D self-rolled biosensor arrays. (2) A 3D confocal microscopy image of 3D cardiac spheroid labeled with Ca^{2+} indicator dye encapsulated by the 3D self-rolled biosensor arrays. (3) Representative field potential traces recorded by the 3D self-rolled biosensor arrays from the 3D cardiac organoid. Adapted with permission [91]. Copyright 2019, The Authors. D) Integrated Pt microelectrodes in a 3D cardiac construct with highly-aligned morphology. (1) Optical image illustrated the arrangement of Pt microelectrodes for electrophysiological recording. (2) Fluorescent image indicated the cardiomyocytes at the part integrated with a Pt microelectrode. (3) SEM image of cardiomyocytes integrated with a Pt microelectrode. (4) Representative extracellular signals recorded from the three Pt microelectrodes. Adapted with permission [92]. Copyright 2023, Elsevier. E) Implantation of mesh nanoelectronics inside 3D cardiac organoids for tissue-wide electrophysiological recording. (1) Optical image of stretchable mesh nanoelectronics. (2) phase images show the deformation of stretchable mesh nanoelectronics by the mechanical forces from organogenesis at different stages. (3) Representative traces recorded from the cardiac cyborg organoid. (4) Isochronal mappings at day 26 and day 35 of differentiation show delays in the activation time. Adapted with permission [94]. Copyright 2019, American Chemical Society.

to that recorded with patch clamp at the same cell simultaneously (Fig. 8F) [103,104].

3.3. Interpreting cardiac contractile activities on the heart-on-a-chip systems

Contractility indicates various properties of cardiac constructs, such as maturation, viability, and morbidity [105,106]. The contractile force, frequency, and synchronization have been commonly applied to evaluate cardiac properties. The measurement of cardiac contractility could be performed on different levels, from single cardiomyocytes to whole organs. For example, atomic force microscopy (AFM) has been applied to detect the beat rate and beat force of a single cardiomyocyte [107]. Ultrasound Cardiogram (UCG) has been used to measure the ejection fraction of a living heart [108]. However, the traditional measurement approaches typically require expensive equipment and labor-intensive procedures and may interfere with the contractility of cardiac tissues. In recent studies, heart-on-a-chip systems have incorporated sensors that enabled convenient on-chip measurements of cardiac contractility. In this section, we summarized heart-on-a-chip systems with the function to measure the cardiac contractility at single cell level, 2D cardiac construct and volumetric cardiac organoids level (Fig. 9A).

Single-cell contractility. For on-chip measurement of the cardiac contractility with single-cell precision, micro-scale transducer structures have been applied to interface with the cardiomyocyte and transform the cell-generated contraction into the deformation of the transducer. A typical form of the platform relies on the array of compliant micropillars with constant controllable dimensions (diameter and height), and the contractions of attached cells bend the micropillars, whose deflections are observed by optical microscopy. Then the contractile forces exerted by cells can be calculated from the displacements of micropillars using beam bending theory. This technique can provide a quantitative force map of cardiomyocytes exerted on each pillar, offering a powerful tool for cardiac contractility studies with a high spatial resolution at the single-cell level. For example, Beussman et al. produced micropillar arrays of PDMS elastomer using soft lithography with a resolution of sub-10 μm, and the correspondence between the deflection of the micropillar and the applied force to the pillar was established. After conducting surface functionalization with extracellular matrix protein to the micropillars, cardiomyocytes were able to adhere atop the micropillars. The deflection of micropillars caused by the in-contact cardiomyocyte was captured by high-speed video microscopy for calculating the contractile force, and the contractile events at each joint point between the cardiomyocytes and nether micropillars can be calculated individually, which indicated the change of contractile force over a single cardiomyocyte. Moreover, this research provided measurement of cardiac contractile force change over a single pulse and demonstrated the pulse duration and time to peak (Fig. 9B) [109,110]. Lee et al. produced mushroom-shaped micropillar arrays, which not only demonstrated the measurement of the contraction force of the cardiomyocyte adhered atop but also the enhancement of cardiac contraction force based on their topography [113]. In addition to the micropillar arrays, micro-cantilevers are another widely applied form of mechanical transducer [114]. For example, Matsudaira et al. designed an on-chip sensor composed of six cantilevers that are 20 μm in width, and 27.5 μm in length that a single cardiomyocyte can cover a cantilever. Direct measurements of the contractile forces generated by the HiPSC-CMs at the frequency of 40 kHz and peak values of several tens of nN were performed, demonstrating high sensitivity and accuracy in measuring the contractile force of cardiomyocytes [115].

2D-cardiac-construct contractility. The contraction measurement of cardiac constructs under 2D culture using mechanical sensors based on the elastic thin film was commonly applied to a heart-on-a-chip model. The 2D cardiac construct was built by culturing cardiomyocytes on an ultra-thin film, and the contraction of the cardiomyocytes can simultaneously induce deflection of the ultrathin film in accordance with the contractile force and frequency. In addition, micro-patterned geometrical or biochemical cues were frequently used to induce spatially ordered 2D myogenesis [116]. In earlier studies, the contraction force and frequency of 2D cardiac constructs can be directly quantified from the motion of the film by analyzing the recorded video [117]. In more recent research, signal-translation parts were induced to the ultra-thin film transforming the film deflection into electrical or optical signals and realizing real-time observation of contraction of 2D cardiac constructs. For example, Kim et al. produced a highly-sensitive crack sensor within a flexible PDMS film, the constant film deflection caused by cardiac contraction induced the real-time opening and closing of the crack, which can be read as the fluctuating resistance by connecting the crack sensor to resistance measuring circuit (Fig. 9C) [111]. Sun et al. prepared electroconductive anisotropic structural color hydrogel film whose color changes with deformation. They proved that the anisotropic morphology of the film could effectively induce the alignment of cardiomyocytes, and the electrical conductivity could contribute to the synchronous beating of cardiomyocytes. Such consistent beating rhythm caused the deformation of the hydrogel substrates and dynamic shifts in structural color and reflection spectra of the whole hybrid hydrogels. Moreover, they demonstrated a visualized heart-on-a-chip system by integrating such cardiomyocyte-driven living structural color hydrogels and microfluidics [118].

3D-cardiac-construct contractility. To study the ventricle pressure and volume dynamics of cardiac tissue on a heart-on-a-chip model, 3D contractile cardiac constructs are required. In theory, cardiomyocytes can be cultured on an elastic chamber structure and the contraction of cardiomyocytes can induce the volumetric variation of the chamber. For example, Abulaiti et al. established a heart-on-a-chip microdevice composed of an opened chamber connected with a micro-channel loaded with fluorescent particles, and a hiPSC-derived 3D cardiac microtissue was sealed on the opening of the chamber. The contraction of the cardiac tissue pumped the fluid in the micro-chamber recapitulating the heart pump function, and the contractile function of the model was evaluated by tracking the displacement of the fluorescent particles [34]. Moreover, MacQueen et al. prepared a 3D fibrous scaffold in the

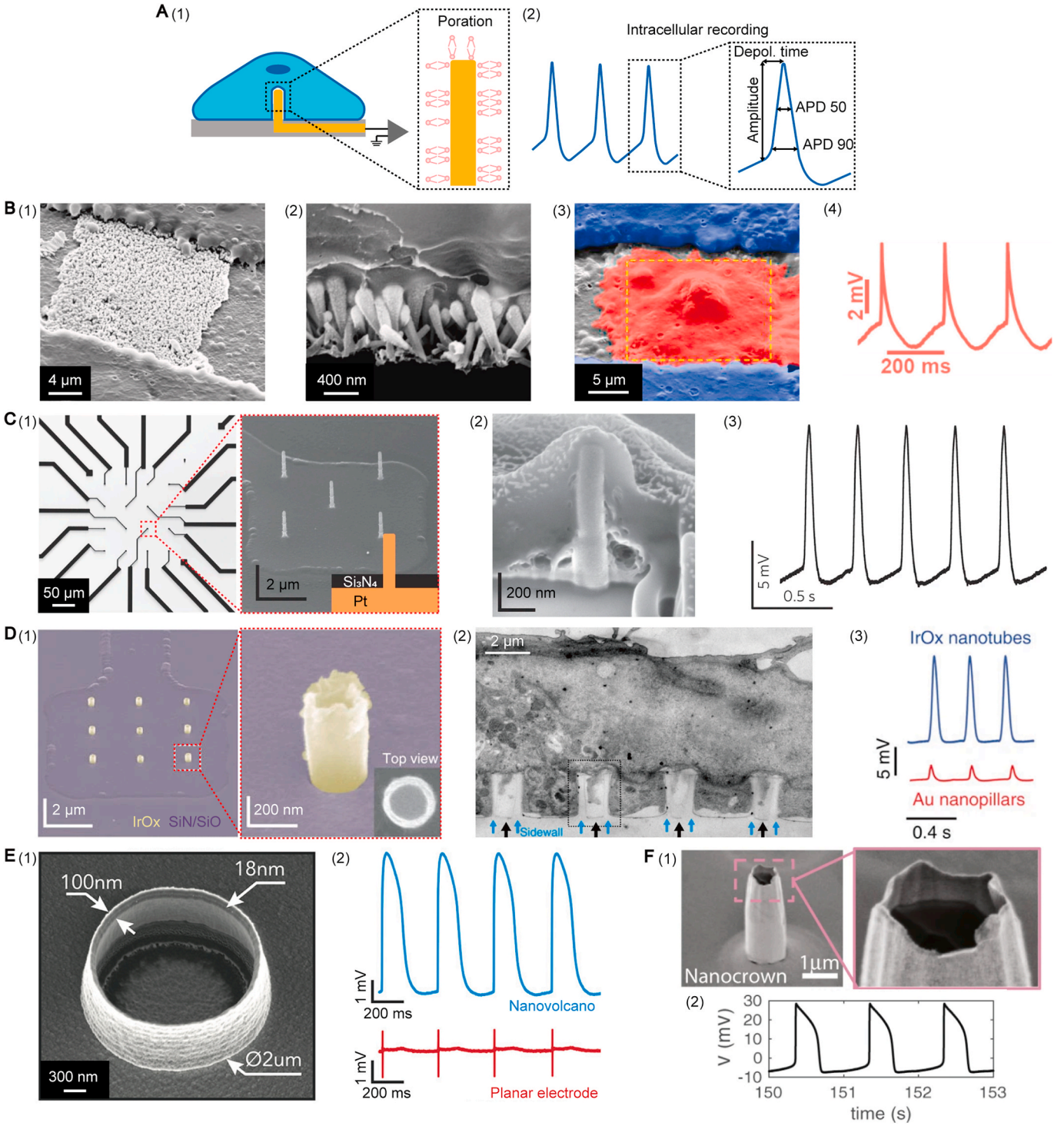

(caption on next page)

Fig. 8. Intracellular electrophysiological recording. A) Schematics depict (1) the spatial relationships between a cardiomyocyte and a 3D microelectrode for intracellular electrophysiological recording, and (2) typical forms of intracellular signals. B) Planar extracellular recording device. B) Nano-branched microelectrode array realized in-cell electrophysiological recording after electroporation. (1–2) Scanning electron microscope (SEM) images of the platinum-coated nanobranches. (3) Colored SEM image of cardiomyocyte (red) on nano-branched microelectrode. (4) Intracellular recording from the primary neonatal rat cardiomyocyte after electroporation. Adapted with permission [98]. Copyright 2020, Elsevier. C) Nano-pillar microelectrode array realized in-cell electrophysiological recording after electroporation. (1) Optical images of a nanopillar electrode device and SEM image of an array of five vertical nanopillar electrodes on one of the platinum pads. (2) The cell-nanopillar electrode interface exposed by FIB milling shows that the nanopillar electrode is fully engulfed by the cell. (3) Representative trace of the intracellular signal recorded from HL-1 cardiomyocyte after electroporation using the nano-pillar electrode array. Adapted with permission [100]. Copyright 2012, Springer Nature. D) Hollow nano-pillar microelectrodes show enhanced electrophysiological recording over nano-pillar microelectrodes. (1) SEM images of an array of IrOx nanotubes on a square Pt pad, and the hollow center of the nanotube can be clearly seen in expanded view. (2) TEM vertical section image of a cardiomyocyte growing on top of quartz nanotube arrays show that the bottom plasma membrane protrudes into the nanotubes. (3) Immediately after local electroporation, both IrOx nanotube and Au nanopillar achieved intracellular recording of action potentials. Adapted with permission [101]. Copyright 2014, Springer Nature. E) Nano-volcano microelectrode arrays realized in-cell electrophysiological recording by membrane fusion. (1) SEM image of the volcano-shaped microelectrode. (2) Intracellular recording of action potentials with a nanovolcano (upper trace) and simultaneously measured electrograms from a nearby planar electrode (lower trace) during spontaneous electrical activity. Adapted with permission [102]. Copyright 2019, American Chemical Society. F) Nanocrown electrode array allows robust recording of intracellular action potentials. (1) SEM image of a nanocrown electrode. (2) Nano-crown electrode arrays measure high amplitude intracellular action potential waveforms after electroporation. Adapted with permission [103]. Copyright 2022, Springer Nature. (For interpretation of the references to color in this figure legend, the reader is referred to the Web version of this article.)

shape of an ellipsoidal chamber and seeded rat or human cardiomyocytes on the scaffold forming a model of the heart ventricle. Notably, the engineered ventricles exhibited *in vivo*-like chamber contraction, the measured differences in chamber pressure were ~50 μmHg (rat or human) and the volume change was ~5 μl (rat) or 1 μl (human), the ejection fractions were ~1 % (rat) or ~0.2 % (human) and stroke work were WS ~0.25 mmHg × μl (rat) or WS ~0.05 mmHg × μl (human) (Fig. 9D) [112].

3.4. Interpreting cardiac biomarkers on the heart-on-a-chip systems

Cardiac biomarkers can provide analytical information critical for understanding the physiological functions, pathological progress, and drug responses of cardiac tissues. These markers are typically cell-secreted proteins to the extracellular environment, such as cytokines, growth factors, and hormones, which carry information involving the status or condition of cardiac tissue. For example, cardiac troponin T and creatine kinase MB (CK-MB) are highly specific biomarkers for assessing ischemic myocardial injury in clinical practice, which can be detected in the blood when a myocardial injury happens [119].

Heart-on-a-chip integrated with aptamer-based electrochemical biosensors can provide noninvasive, accurate information on the status of cardiac constructs at low working volumes. For a typical aptamer-based electrochemical biosensor, the analyte-binding event is indicated by electrochemical current variations (Fig. 10A) [120]. For example, Shin et al. reported a microfluidic aptamer-based electrochemical sensing platform with microelectrode functionalized with aptamers that are specific to CK-MB biomarkers secreted from damaged cardiac tissue. To perform the detection of biomarkers, the platform was connected with a heart-on-a-chip model, and the measurement of CK-MB secreted by the cardiac organoids upon a cardiotoxic drug, doxorubicin, in a dose-dependent manner was demonstrated (Fig. 10B) [121]. In addition, by detecting the secretion rate of cardiac biomarkers the interactions between cardiac tissue with other tissues can be reflected. For example, Lee et al. presented a heart-on-a-chip platform consisting of healthy/fibrotic cardiac tissue and breast cancer tissue, demonstrating that the communications between healthy/fibrotic cardiac and BC cells significantly altered the secretion rate of biomarkers, Troponin T and HER-2 (Fig. 10C) [122].

4. Typical biomedical applications of heart-on-a-chip systems

The above discussion reveals that heart-on-a-chip systems hold great promise to reflect the key structures of native cardiac tissue, promote the maturation of *in vitro* cardiac microtissues, and detect the condition of on-chip cardiac constructs, which can support intelligent cardiac studies. In this section, we discuss various applications of heart-on-a-chip for intelligent cardiac studies, including cardiac physiological research, pathological research, and pharmacological assessment.

4.1. Heart-on-a-chip systems for cardiac physiological studies

Heart-on-a-chip systems provide online monitoring and control over the functionalities of *in vitro* cardiac models, enabling researchers to understand the physiology of the human heart in depth [123,124]. For instance, heart-on-a-chip systems equipped with high-resolution sensors enable the monitoring of single-cell activities, which can provide a detailed understanding of the development and mechanism of the human heart [125,126]. Liu's group developed a heart-on-a-chip system with nano-scale electrophysiological sensors that can non-invasively integrate with on-chip cardiac tissues. By culturing a 3D organoid composed of hiPSC-CMs in the system, they performed tissue-wide integration between the electrophysiological sensors and the 3D heart-like structure. The intimate contact between the sensors and cells enabled the real-time recording of multi-site electrophysiological signals from the 3D human cardiac model, offering chronic and systematic observation of the development, propagation, and synchronization of the human cardiac tissue (Fig. 11A) [94]. In addition, the heart-on-a-chip systems offered dynamic modulation of the culture conditions, mimicking the specific stage of heart development can be realized. For example, Kolanowski et al. developed a heart-on-a-chip system and cultured hiPSC-CMs, and revealed the structural and functional maturation of the hiPSC-CMs at an early stage. The heart-on-a-chip system enabled dynamic force stimulation and on-demand oxygen supply, increasing cell alignment and contractility of the hiPSC-CMs observed during a one-week culture. In addition, the dynamic culture condition proposed the growth of hiPSC-CMs, and increased the cell size and sarcomere length compared with the well-plate-based static culture (Fig. 11B) [127].

4.2. Heart-on-a-chip systems for cardiac pathological studies

Heart-on-a-chip systems can provide tunable approaches to accurately alter the condition of on-chip cardiac tissue and the culture environment, and have been used to mimic the course of heart-related diseases, such as arrhythmia, fibrosis, myocardial infarction, etc. [27,128]. Arrhythmia is defined as any pathological irregularity in either the heart rate or rhythm, which is commonly caused by the interruption of electrical signal propagation through the cardiac conduction system [129]. To reproduce human cardiac arrhythmias on a heart-on-a-chip system, Williams et al. developed on-chip 3D cardiac tissue of hiPSC-CMs and induced arrhythmia by adding methyl-beta cyclodextrin to disassemble the gap junctions between cardiomyocytes. The model recapitulates key aspects of complex arrhythmias *in vitro*, including the

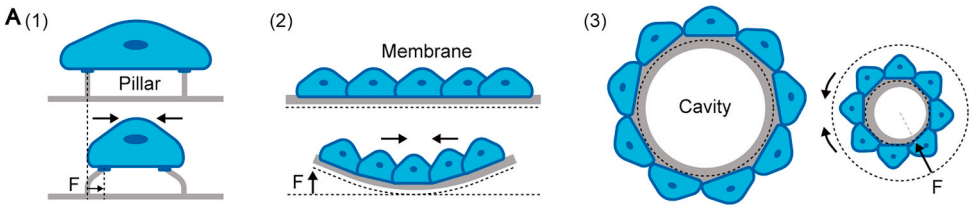

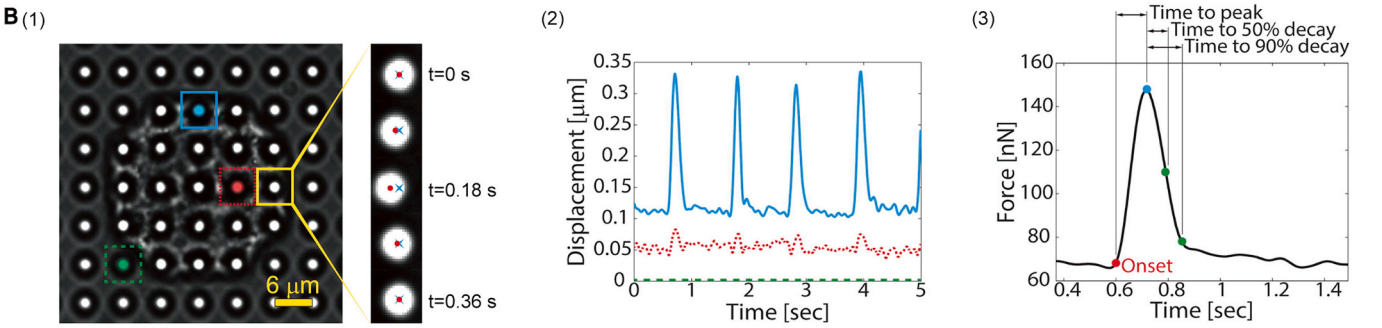

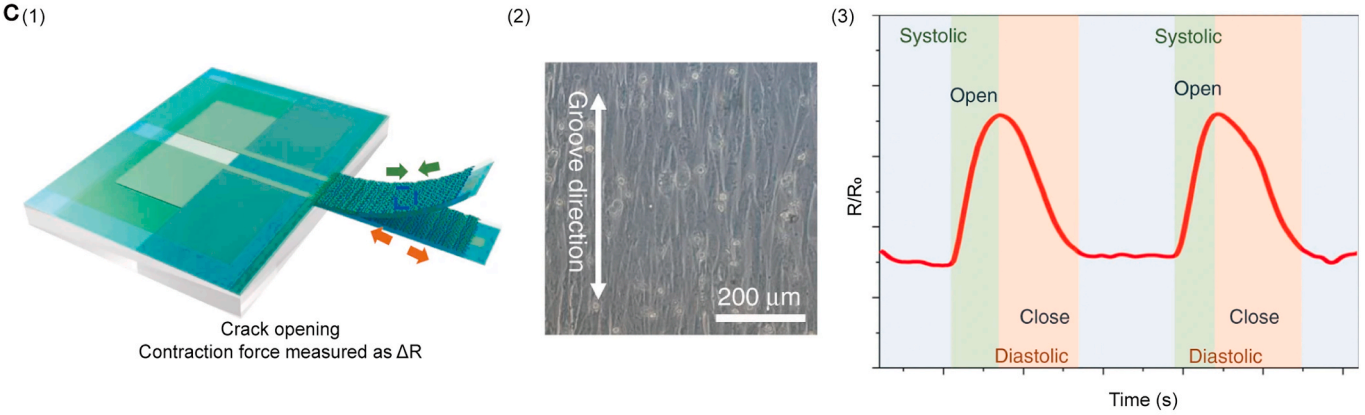

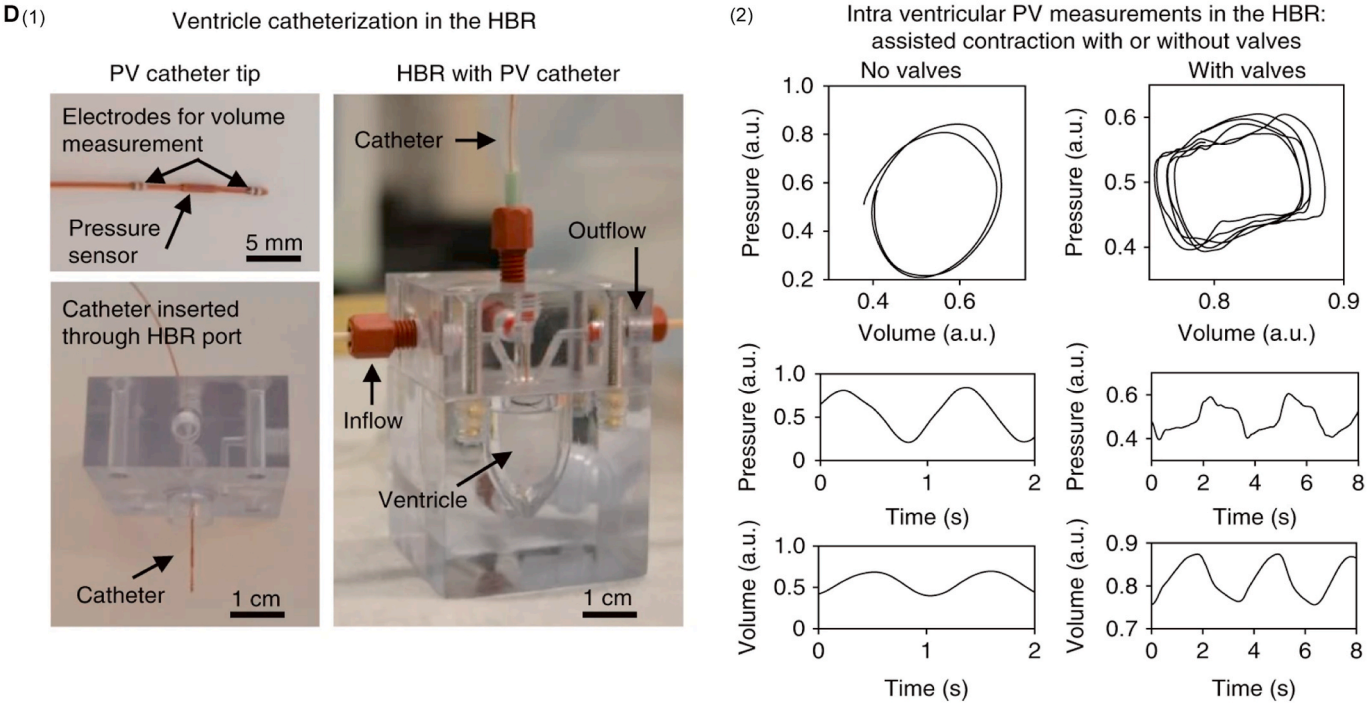

(caption on next page)

Fig. 9. Sensing of cardiac contract force. A) Schematics illustrate the measurement of cardiac contractility at (1) single cell level, (2) 2D cardiac construct, and (3) volumetric cardiac organoids level. B) Measuring the contract force of cardiomyocytes using a deformable pillar. (1) Phase contrast image of a cardiomyocyte on micro-posts and the displacement of a micro-post. Adapted with permission [109]. Copyright 2014, Elsevier. (2) For each micro-post, the deflection is calculated at each frame to produce a waveform. Posts near the edge of the cell (blue) typically deform much more than posts near the middle (red). (3) The calculated force waveform from a single contraction from the cardiomyocyte and the characteristic times. Adapted with permission [110]. Copyright 2016, Elsevier. C) Measuring cardiac contractility by membrane cantilever integrated with a PDMS-encapsulated crack sensor. (1) Schematic of a silicone rubber cantilever for measuring the contractile force of cardiomyocytes. (2) Nano-patterns used to align the cardiomyocytes on the cantilever surface. (3) Representative trace of real-time change in resistance ratio. Adapted with permission [111]. Copyright 2020, Springer Nature. D) Cardiac contractility measurement based on tissue-engineered model ventricles. (1) Ventricle catheterization in the heart bioreactor (HBR). (2) Pressure and volume measurements during assisted ventricle contraction with or without cast-molded silicone tricuspid valves. Adapted with permission [112]. Copyright 2018, Springer Nature. (For interpretation of the references to color in this figure legend, the reader is referred to the Web version of this article.)

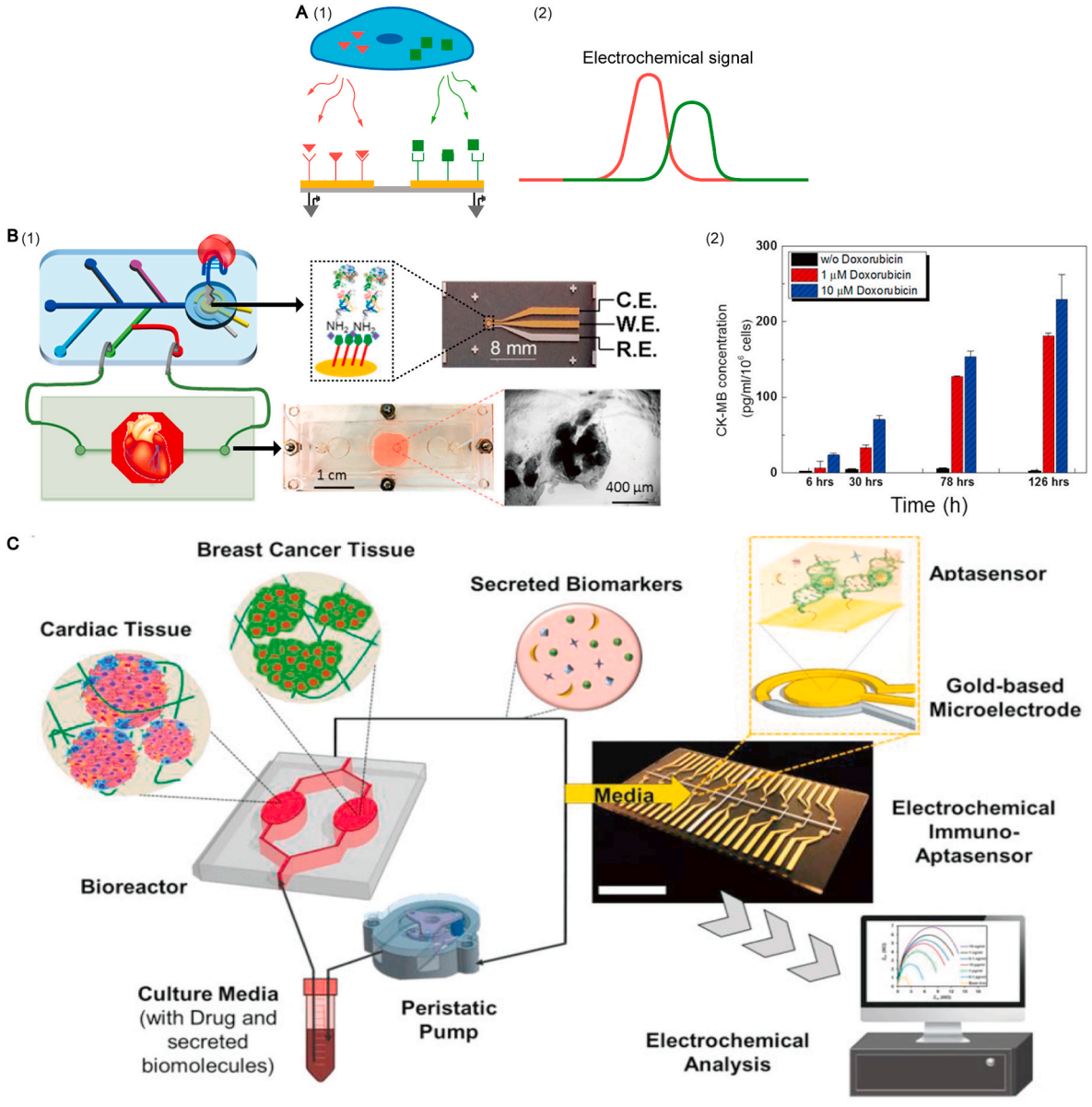

Fig. 10. Sensing of cardiac biomarkers. A) Schematics illustrate (1) the analyte-binding event on a typical aptamer-based electrochemical biosensor and (2) electrochemical current variations. B) Aptamer-based microfluidic electrochemical biosensor for monitoring cardiac biomarkers. (1) Schematic and photograph of the microfabricated electrode set in a microfluidic bioreactor. (2) Calculated CK-MB concentrations obtained using the calibration curve. Adapted with permission [121]. Copyright 2016, American Chemical Society. C) A heart-breast cancer on-a-chip platform with electrochemical sensors for monitoring cell-secreted multiple biomarkers. Adapted with permission [122]. Copyright 2021, WILEY-VCH.

asynchronous beating and 3D differential propagation of electrophysiological signals [130] (Fig. 12A). Myocardial fibrosis is generally caused by abnormal proliferation of cardiac fibroblasts and a significant increase in collagen deposition in myocardium, which imbalances the ratio of functional cardiomyocytes and disrupts the diastolic function of the heart [131]. To model myocardial fibrosis *in vitro*, Wang et al. developed a heart-on-a-chip system by artificially changing the hiPSC-CMs to cardiac fibroblast (CFs) ratio of the on-chip 3D cardiac

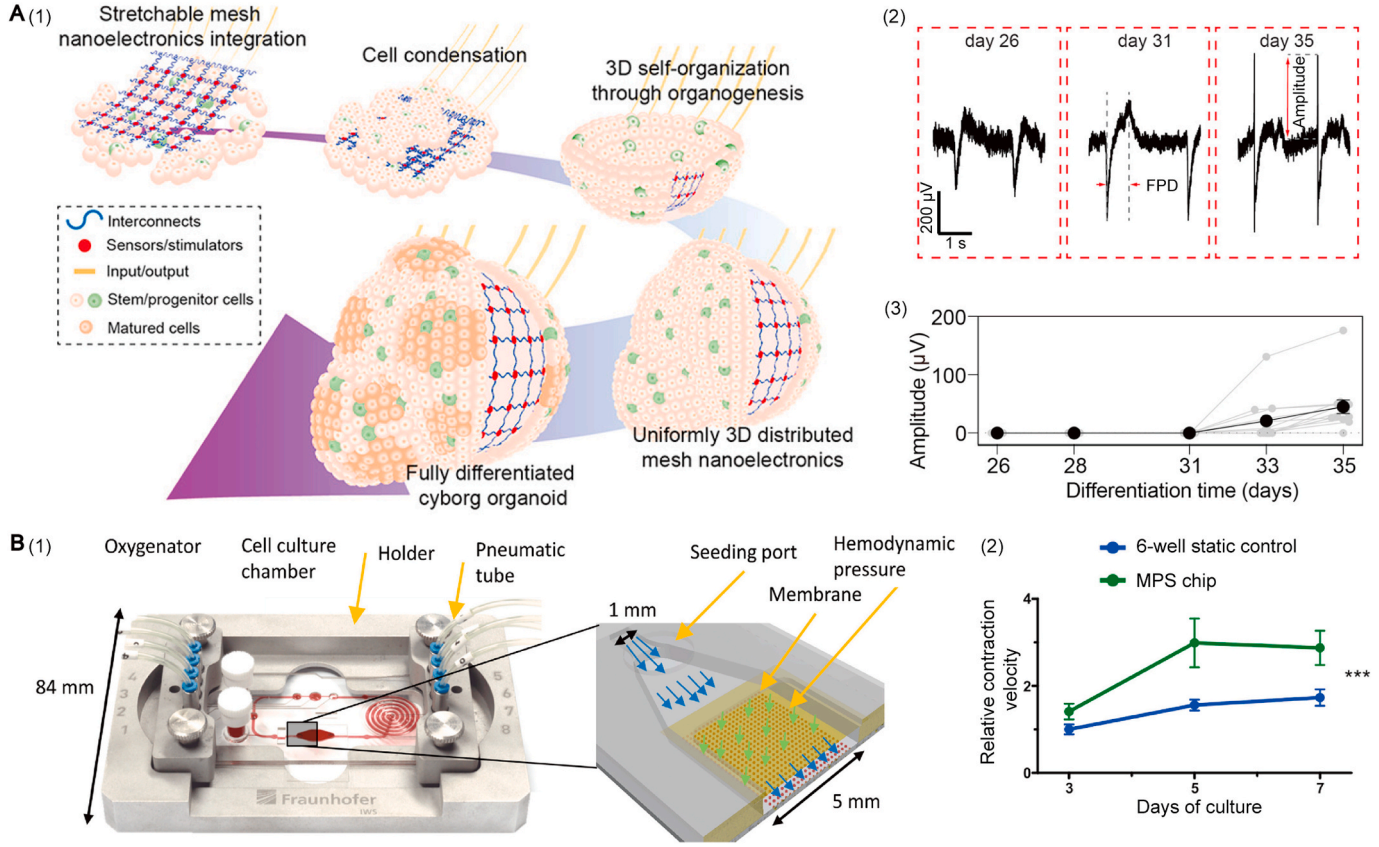

Fig. 11. Heart-on-a-chip for understanding the physiological processes of cardiac constructs. A) Heart-on-a-chip model for understanding the time-dependent tissue-wide electrophysiological activity of 3D cardiac organoids. (1) Schematics illustrate the stepwise integration of stretchable mesh nanoelectronics into organoids through organogenesis. (2) Zoom-in views of extracellular signal on three different culturing days (days 26, 31, and 35 of differentiation). (3) Amplitude of fast peak as a function of differentiation time. Adapted with permission [94]. Copyright 2019, American Chemical Society. B) On-chip observation of contractility changes of cardiomyocytes during culture. (1) Image of the complete microdevice fixed in a holder. (2) Increased contraction velocity of cultures in MPS chips compared to 6-well static controls. Adapted with permission [127]. Copyright 2020, Elsevier.

tissue. This model used 1:3 CMs to CFs to model the fibrotic tissue and 3:1 C M to CF condition as the normal control. An interstitial fibrotic phenotype with decreased contractile function and pathological collagen deposition was observed in the fibrotic tissue, and the Ca^{2+} transients showed an impaired excitation-contraction coupling phenotype, indicating that the heart-on-a-chip system can model the fibrotic cardiomyopathy in the adult human heart [132]. Myocardial infarction commonly arises from the interruption of blood supply to a part of the heart, and the ensuing oxygen shortage can cause damage or even death of the cardiac muscle tissue [133,134]. Ren et al. described a heart-on-a-chip system mimicking hypoxia-induced myocardial injury by perfusing the anoxic reagent, FCCP solution, to the on-chip cultured H9C2 cardiac cells. The pathological fluidic condition of the extracellular microenvironments in the myocardial tissue induced significant apoptosis effects on the myocardial cells, such as cell shrinkage, disintegration of the cytoskeleton, loss of mitochondrial membrane potential, and caspase-3 activation [135,136] (Fig. 12B). Furthermore, heart-on-a-chip systems equipped with biosensors can offer real-time readouts, which enabled the understanding of rapid changes that occur during specific cardiac injury. For example, Liu et al. demonstrated a heart-on-a-chip system equipped with a microfluidic channel that enabled temporal modulation of medium oxygenation and Pt-nanopillar electrodes to study the effects of acute hypoxia on cardiac function. The model provided continuous and multiplexed measurements of action potentials (APs) during the induction of hypoxia, and they found that hypoxic cells experienced an initial period of tachycardia followed by a reduction in beat rate and eventually arrhythmia, and the propagation of action potentials between cardiomyocytes was in turbid patterns. In addition, the APs were narrowed during hypoxia, consistent with proposed mechanisms [137] (Fig. 12C).

4.3. *Heart-on-a-chip systems for cardiac pharmacological studies*

Heart-on-a-chip systems offer non-invasive and label-free detection of cardiac response under the treatment of drugs that target cardiac electrophysiological activity and contractility. We summarized the pharmacological effects of typical cardiac-related drugs and experimental results from heart-on-a-chip systems (Table 1).

Cardiac-related pharmacological components commonly act on the ion channels of cardiomyocytes, which can alter the ion flow across the cell membrane. According to the different effects of the component, the electrophysiological signals generated by the cardiomyocyte exhibit different phenotypes (Fig. 6). Heart-on-a-chip systems with sensors for recording cardiac electrophysiological signals can monitor the electrophysiological signal in real-time, providing effective methods to interpret the effect of the pharmacological components. For example, dofetilide is an effective potassium channel blocker and was proven to prolong the repolarization time measured from the epicardial electrogram of an *in vivo* animal model [141]. Yang et al. exerted dofetilide on a heart-on-a-chip system with 3D nanocrown-shaped electrodes. The in-cell recording results showed that the APD90 of the intracellular signal increased after the treatment of dofetilide at the concentration of 0.3–3 nM. Since the APD90 is approximately equal to the repolarization time, the effect of dofetilide is consistent in the *in vivo* animal model and the *in vitro* heart-on-a-chip system [104] (Fig. 13A).

The heart-on-a-chip system with strain sensors was applied to detect

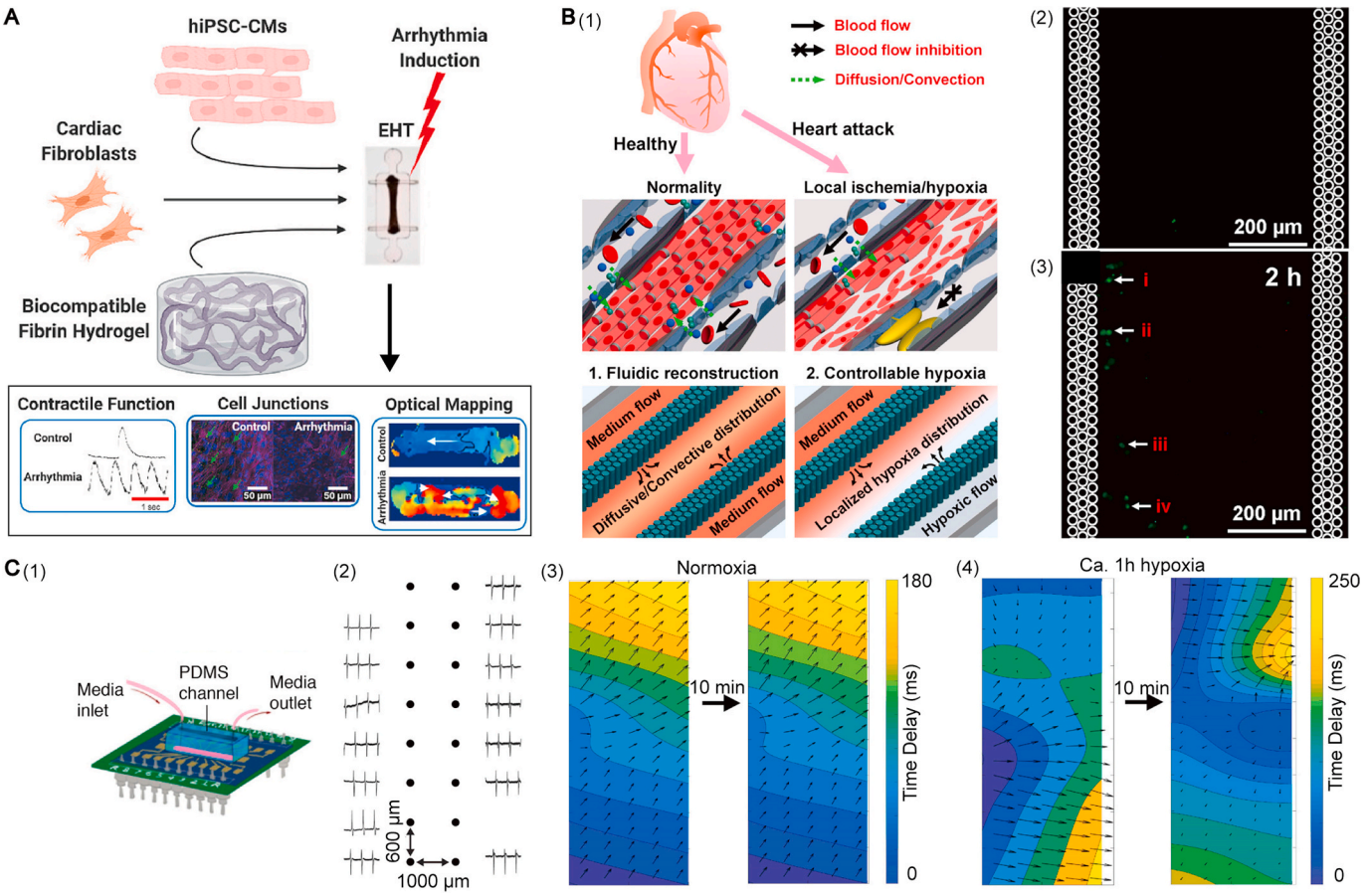

Fig. 12. Heart-on-a-chip for understanding the pathological processes of cardiac constructs. A) Heart-on-a-chip model with 3D engineered heart tissue (EHT) of hiPSC-CMs demonstrating arrhythmias in contractility, cell-cell junction, and electrophysiological conduction. Adapted with permission [130]. Copyright 2021, Elsevier. B) Investigation of hypoxia-induced myocardial injury dynamics in a tissue interface mimicking microfluidic device. (1) Schematic diagrams of the microfluidic device for studying controllable myocardial hypoxia and for the myocardial fluidic microenvironment mimicking. (2) Fluorescence image of the caspase-3+ cells in the chamber before hypoxia treatment. (3) Fluorescence image of the caspase-3+ cells in the chamber after 2-h hypoxia treatment, indicating the caspase-3 activation of myocardial cells. Adapted with permission [135]. Copyright 2012, American Chemical Society. C) Heart-on-a-chip model with integrated bioelectronics for monitoring cardiac electrophysiology under acute hypoxia. (1) Scheme representing fully assembled chip with integrated recording elements, reference electrode, and PDMS channel for media delivery. (2) Scheme of electrode layout and representative multiplexed readouts from a chip with 14 out of 16 functional bioelectronic interfaces. (3–4) Isochronal maps representing signal propagation at two time points each during normoxia and hypoxia for about 1 h. Adapted with permission [137]. Copyright 2020, American Chemical Society.

the pharmacological effect of drugs targeting cardiac contractile functions. For example, isoproterenol and verapamil are proven to have stimulating and inhibiting effects on heart contractility in clinical use, respectively. An *in vivo* study showed that the intravenous administration of isoproterenol in men in a dose of 0.063 and 0.44 μg/kg increases the heart rate by 15 and 30 beats/min, respectively. Conversely, the intravenous administration of verapamil in man in decreases the heart rate. Researchers have applied the two drugs in heart-on-a-chip systems to examine their effect on the contractility of *in vitro* cardiac models. Lind et al. introduced a heart-on-a-chip system equipped with soft strain gauge sensors, and cultured laminar cardiac tissue composed of NRVMs and hiPSC-CMs. Isoproterenol treatment showed a similar dose-dependent increase of cardiac contractility stress on laminar NRVM tissue (EC_{50} = 1.2 nM, under 1.5 Hz pacing) and hiPS-CM-based laminar tissue (EC_{50} = 2.7 nM, under 2 Hz pacing). Verapamil treatment on laminar NRVM tissue showed a dose-dependent decrease of contractile stress (EC_{50} = 790 nM, under 1.5 Hz pacing) [42] (Fig. 13B). Similarly, Sun et al. developed a heart-on-a-chip with a microgroove structure for developing aligned laminar NRVM tissue and a sensor for real-time readout of the strain caused by the cardiac tissue. Isoproterenol treatment showed a dose-dependent increase in contractility stress (EC_{50} = 92.6 nM) and beating rate (EC_{50} = 71.4 nM). Verapamil treatment showed a dose-dependent decrease in cardiac contractility stress (EC_{50} = 802.9 nM) and beating rate (EC_{50} = 921.0 nM), both EC_{50} values were close to the previously reported data of rat heart [146,148].

In addition, rather than directly targeting the heart, some pharmacological components were found to induce the production of secondary factors that act on heart function during the circulatory and metabolic processes. For instance, cyclophosphamide is a known drug that relates to cardiac function depending on hepatic metabolism. The mechanism of cyclophosphamide-driven influence on cardiac function is not fully understood, but findings implicate the production of the metabolite acrolein through liver metabolism, which was proved to alter cardiac function and signaling in *vivo* tests [153]. This indirect effect of pharmacological components involves the heart and other interconnecting tissue units, which cannot be reflected using a heart-on-a-chip system with cardiac tissue only. In recent years, researchers have made efforts to understand the indirect effect of interconnecting cardiac tissue with other organ modules in a heart-on-a-chip system. For example, Oleaga et al. developed a heart-on-a-chip system containing hiPSC-CMs and primary hepatocytes for the study of cardiotoxicity upon hepatic metabolism. The heart-on-a-chip system allows tracking of cardiac electrophysiological and contractile functions while perfusing pharmacological components passing through the on-chip liver and cardiac

Table 1
The pharmacological effects of typical cardiac-related drugs and experimental results from heart-on-a-chip systems.

Drug	General effect	Results from *in vivo* human/animal or pharmacological study	Cell in heart-on-a-chip system	Results from heart-on-a-chip systems	Reference
Quinidine	Potassium channel blocker	Cause dose-dependent reduction of the peak amplitude of $I_{k(f)}$ (K_d = 41 μM); Inhibit the I_{Kr} about 80 % at 5 μM	HiPSC-CMs	Prolong the cAPD90 significantly at 10 μM; Show little effect on the cycle length at 10 μM	[104, 138–140]
Dofetilide	Potassium channel blocker	Increase the activation-repolarization interval of the adult beagle dog model between 3 μg/kg and 100 μg/kg	HiPSC-CMs	Increase the APD90 between 300 pM and 3 nM; Decrease the cycle length between 300 pM and 3 nM	[104,141]
Lidocaine	Sodium channel blocker	The half-blocking concentration of cardiac sodium channels varied from about 300 μM to 10 μM	HiPSC-CMs	Increase the cycle length significantly at 100 μM; Decrease the cAPD90 slightly at 100 μM	[104,142, 143]
Flecainide	Sodium channel blocker	Prevent exercise-induced ventricular tachycardia in mice at about 2.5 μM	HiPSC-CMs	Increase the cycle length at 3 μM; Affect the cAPD90 minimally at 3 μM	[104,144, 145]
Isoproterenol	Positive inotropic responses	Increase the heart rate of the human by 15 beats/min (at 63 ng/kg) and 30 beats/min (at 440 ng/kg) after intravenous administration; Increases the heart rate of the dog model by 22 beats/min (at 270 ng/kg) and 80 beats/min (at 640 ng/kg) after intravenous administration	NRVMs	Increase the contractile stress in a dose-dependent manner between 10 pM and 10 μM (EC_{50} = 92.6 nM); Increase the beating rate in a dose-dependent manner between 10 pM and 10 μM (EC_{50} = 71.4 nM)	[8,42,146, 147]
			Laminar NRVM tissue	Increase the contractile stress in a dose-dependent manner between 10 pM and 10 μM (EC_{50} = 1.2 nM)	
			Laminar hiPSC-CM tissue	Increase the contractile stress in a dose-dependent manner between 10 pM and 10 μM under (EC_{50} = 2.7 nM)	
			3D hiPSC-CM tissue	Increase the contractile frequency and force at 1 μM and 5 μM	
Verapamil	Negative inotropic responses	Cause dose-dependent reduction of the contractile force of the rat heart (IC_{50} = 170 nM); Decrease the heart rate of the human after intravenous administration	Laminar NRVM tissue	Decrease the contractile stress in a dose-dependent manner between 100 pM and 100 μM (EC_{50} = 790 nM);	[42,146,148, 149,150]
			NRVMs	Decrease the contractile stress in a dose-dependent manner between 1 pM and 1 μM (EC_{50} = 802.9 nM); Decrease the beating rate in a dose-dependent manner between 1 pM and 1 μM (EC_{50} = 921.0 nM)	
Propranolol	Negative inotropic responses	Nonselective β-adrenergic receptor antagonist, with high affinity for the β1AR (K_i = 1.8 nM) and β2AR (K_i = 800 pM)	3D hiPSC-CM tissue	Increase the contractile frequency and force at 1 μM and 5 μM	[8,151]
Norepinephrine	Positive inotropic responses	Show affinity for α2A receptor (K_i = 56 nM) and α1 receptor (K_i = 330 nM)	HiPSC-CMs	Increase the field potential and contractility at 400 nM	[21,152]

units. Experimental results indicated that the cyclophosphamide (9 mM) significantly reduced cardiac conduction velocity, spontaneous beat frequency and contractile force by ~62.2 %, 93.2 %, and 80.8 %, respectively in the presence of hepatocytes [154] (Fig. 14A). Skardal et al. developed a heart-on-a-chip with cardiac, lung and liver organoids integrated in a closed circulatory perfusion system. Bleomycin was infused into the heart-on-a-chip system, which was demonstrated to cause significant lung inflammation, inducing the generation of inflammatory marker interleukin-1β that has cardiotoxicity *in vivo* [155]. The results show that bleomycin did not cause cessation of cardiac organoid beating but the cardiac organoids cultured in the system ceased beating obviously, consistent with the indirect toxic effect on cardiac tissue [156] (Fig. 14B).

5. Conclusions and outlooks

In this review, we summarized the requirements and techniques for producing heart-on-a-chip systems to become an effective and accurate method in cardiac studies. Specifically, we discussed the basic fabrication techniques for engineering heart-on-a-chip systems. Furthermore, we analyzed the necessity for engineered heart-on-a-chip systems with biomimetic and sensing functions. We summarized the methods to construct cardiac tissues *in vitro* with characteristics close to the native heart and acquire physiological information from on-chip cardiac constructs. In addition, we shed light on the typical applications of heart-on-a-chip in cardiac studies. Nowadays, the development of heart-on-a-chip systems is still in the ascendant, and progress can be made in systematization, integration, and maturation.

Systematization. The human heart is a systematically organized organ, which can be interpreted by the internal construction of the heart and the external connection between the heart and other organs. In terms of internal construction, the heart is composed of organized multiple cells that are organized hierarchically. As a result, for the construction of heart-on-a-chip systems, it is necessary to mimic the native composition and organization of native cells and construct a 3D cardiac construct with a hierarchical structure. The main challenge is accurately assembling different kinds of cells within a 3D cardiac construct in proper positions, and in addition, the co-culture of multi-kinds of cells needs to be further resolved. Aiming at this, 3D bioprinting may be an effective solution since this technique excels at arranging cell-loading inks in a free-form manner, and it will likely see advances in morphogenesis that involve multiple cells, biochemical cues and matrix recapitulating the shape and composition of native cardiac tissue [157]. For external connection, the heart is in connection with other tissues/organs by import/export vessels, innervated by sympathetic and vagus nerves, and interactive with surrounding environments. One effective method to systematically interconnect on-chip cardiac constructs and other tissues is producing 'X-on-a-chip' models individually and assembling those modular and automated micro-environment controllers with organized micro-channels, as reported by Ali

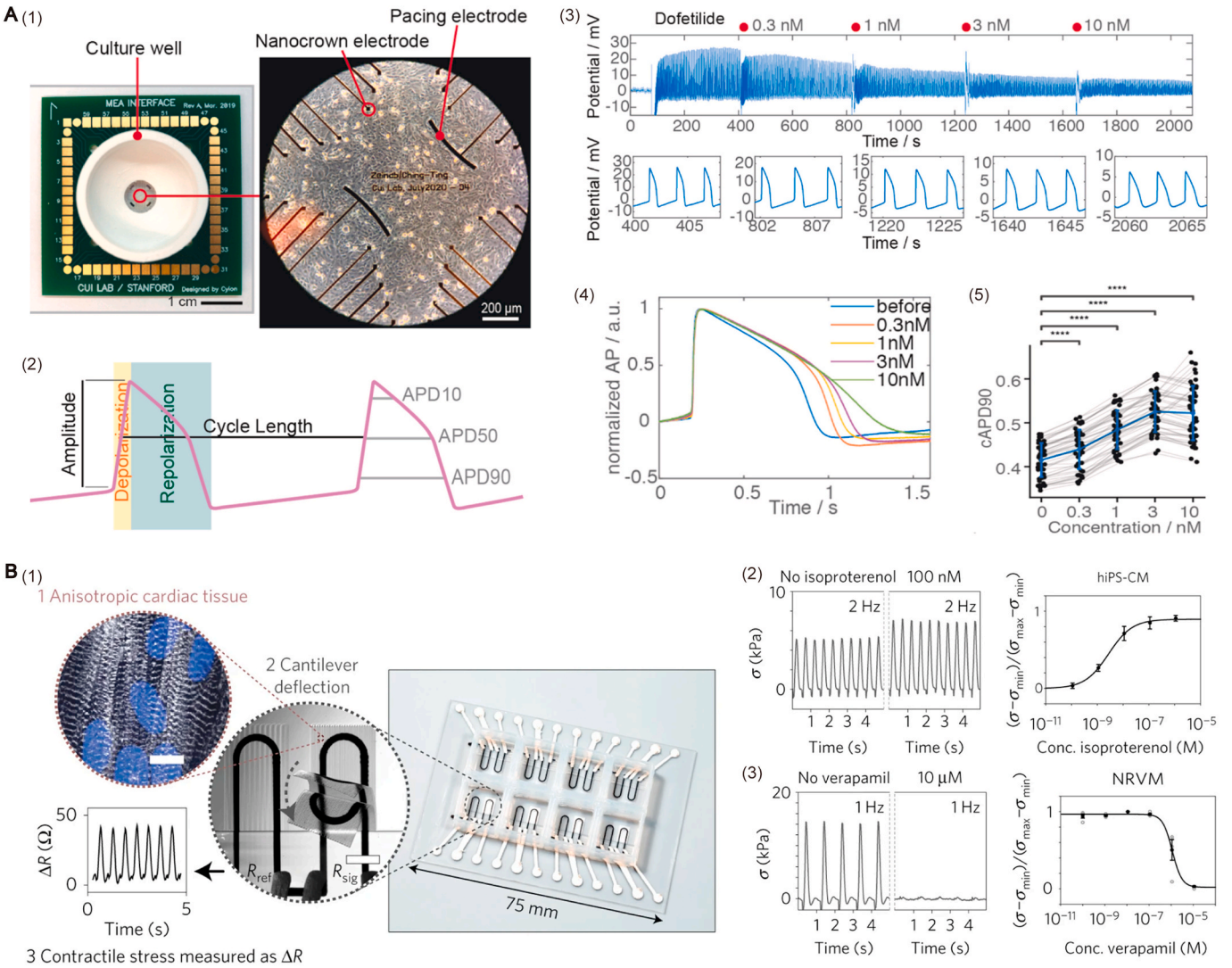

Fig. 13. Heart-on-a-chip for pharmacological study. A) Assessment of pharmacological compounds by intracellular cardiomyocyte electrophysiological signals. (1) Heart-on-a-chip with nanoelectrodes for intracellular electrophysiological signal monitoring. (2) Illustration of the characteristic features of intracellular electrophysiological signal. (3) Representative intracellular electrophysiological signals with multi-dose dofetilide administrations. (4) Overlaid intracellular signals before and after different doses of dofetilide. (5) Quantifications of the cAPD90 with increasing concentrations of dofetilide. Adapted with permission [104]. Copyright 2022, Elsevier. B) On-chip assessment of drugs' work on cardiac contractility. (1) Heart-on-a-chip with aligned laminar cardiac tissue and integrated strain sensor. (2) Representative traces of twitch stress generated by a laminar NRVM tissue when tissue is exposed to verapamil and the corresponding dose–response curve. (3) Representative traces of twitch stress generated by a laminar hiPS-CM tissue when exposed to isoproterenol and the corresponding dose–response curve. Adapted with permission [42]. Copyright 2017, Springer Nature.

Khademhosseini group [19]. Further efforts on improved scaling of this kind of platform should allow for more accurate modulating of on-chip tissues and modeling of the human system.

Integration. The physiological activity of the heart is accompanied by multiple signals, generally including biological, mechanical, electrical, and morphological cues. To holistically interpret the condition and response of a cardiac construct in cardiac physiological, pathological, and pharmacological studies, it is necessary to acquire multimodal signals from on-chip cardiac constructs contemporaneously. On a heart-on-a-chip model, this can be implemented by integrating multimodal sensors on one chip, which calls for advanced design and fabrication techniques. Efforts have been made to produce multimodal sensors for cardiac study. Rogers group developed a 3D multifunctional integumentary mesh electronic for spatiotemporal cardiac measurements, and they integrated an electrophysiological sensing electrode, mechanical strain gauge, pH, and temperature sensors on one device. The function of this multifunctional device was demonstrated by *in vitro* multimodal detection on isolated rabbit hearts [158]. However, the reported device targets measuring multimodal signals on a whole organ, which is not suitable for miniaturized on-chip cardiac constructs. To detect multimodal signals from on-chip cardiac constructs, Qian et al. developed a novel cardiac platform that can record cardiac cell adhesion, electrophysiology, and contractility on the same chip, but this device is limited to detecting 2D cardiac tissues. Suitable devices and methods for integrating multimodal sensors on heart-on-a-chip systems are still in demand.

Maturation. In the diagnosis and treatment of cardiac-related diseases, there is substantial interpersonal variability. As a result, heart-on-a-chip systems capable of interpreting the physiological state of the cardiac construct for individual persons are in demand. To produce customized heart-on-a-chip systems, it is necessary to build cardiac tissues based on personal-specific cells. Notably, the development of hiPSC-CMs has laid the foundations to fulfill this requirement [159]. Generally, by taking the stem cells from patients and differentiating them into CMs, it is possible to model specific diseases and personalized medicine. However, the hiPSC-CMs commonly show immature

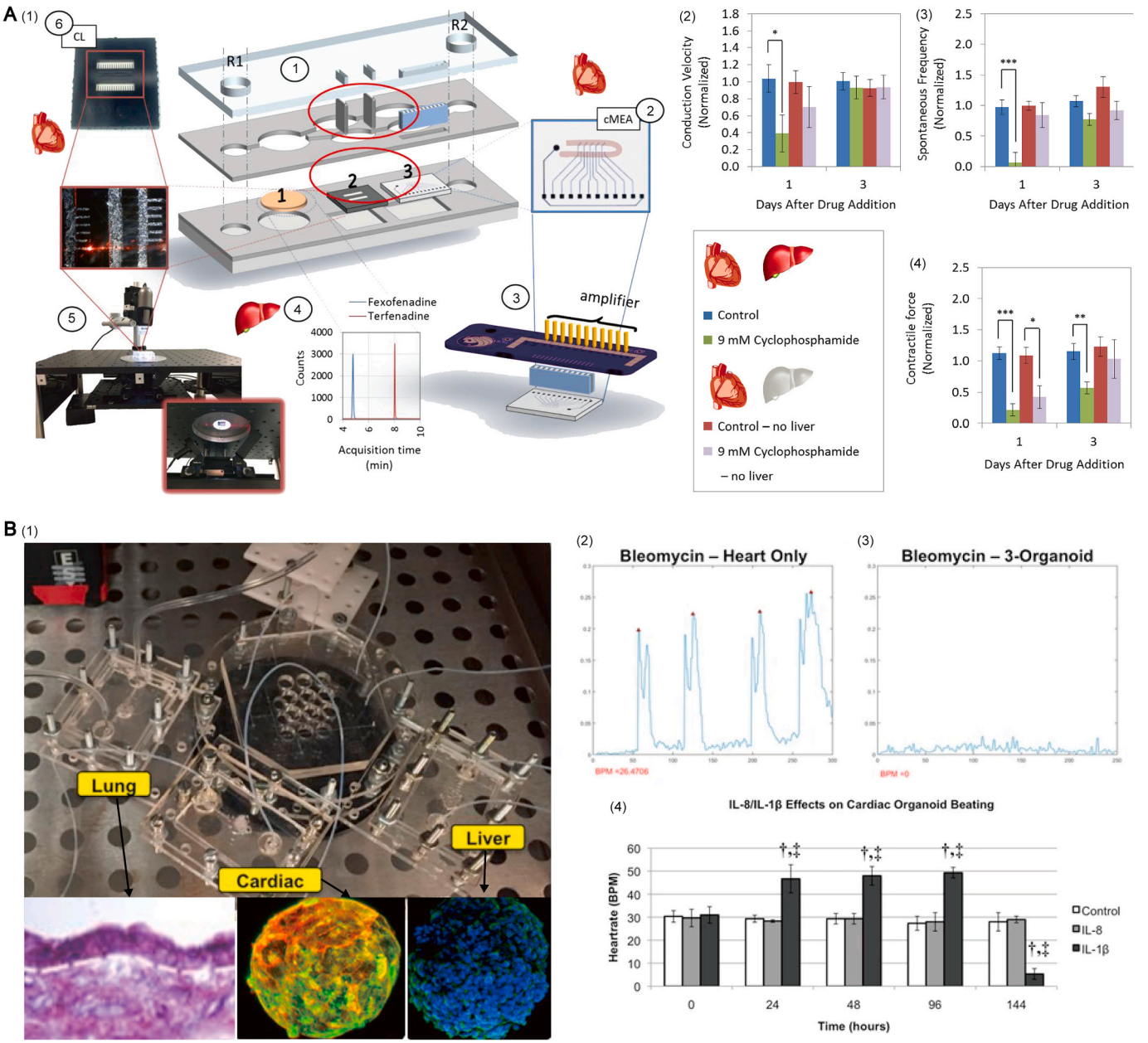

Fig. 14. Heart-on-a-chip systems involve the heart and other interconnecting tissue units for studying the indirect effect of pharmacological components on cardiac tissue. A) Heart-on-a-chip system containing heart and liver units to study the indirect effect of pharmacological components. (1) Cardiac and liver co-culture in a pumpless microfluidic system. Inset 1: the microfluidic flow pathway and the compartments for the system. Inset 2–3: cardiomyocytes cultured on the integrated MEAs. Inset 4: drug compound quantification in the system. Inset 5–6: cardiomyocytes cultured on the integrated cantilevers. Heart-liver system and cardiac outcome upon cyclophosphamide treatment, including (2) cardiac conduction velocity, (3) spontaneous beat frequency, and (4) contractile force. Adapted with permission [154]. Copyright 2018, Elsevier. B) Cardiac-liver-lung interactions in an interconnected system. (1) Photograph of the modular multi-tissue organ-on-a-chip hardware system set up for maintenance of 3-tissue models. (2) Cardiac organoid beating plots of isolated cardiac organoids, bleomycin did not cause a cessation of beating. (3) Cardiac organoid beating plots of cardiac organoids cultured in the system, showed ceased beating completely under bleomycin treatment. (4) Results indicating IL-1β induces an initial increase, followed by a significant decrease in the beating rate of the cardiac organoid. Adapted with permission [156]. Copyright 2017, The Authors.

functional characteristics with embryonic and fetal tissue attributes that can serve as good models for cardiac developmental and early-onset disease studies but cannot adequately mimic late-onset disease and mature tissue [160,161]. It remains questionable whether these models can reflect the pharmacological aspects of a fully developed heart enough to draw clinically relevant conclusions. In recent research, it has been reported that the long-term culture, mechanical, and electrical stimuli enable the maturation of hiPSC-CMs [63,162,163]. Heart-on-a-chip systems provided the advantage of long-term dynamic culture with controlled medium flows and components, as well as offering mechanical and electrical stimuli in a programmable manner. Further study is expected to establish heart-on-a-chip systems based on matured hiPSC-CMs with age-dependent phenotypes for the replication of physiological, pathological, and pharmacological aspects of the fully developed heart *in vitro*.

CRediT authorship contribution statement

Bingsong Gu: Conceptualization, Investigation, Writing - original draft, Writing - review & editing. **Kang Han:** Conceptualization, Investigation, Writing - original draft. **Hanbo Cao:** Conceptualization, Investigation. **Xinxin Huang:** Writing - original draft. **Xiao Li:** Conceptualization, Funding acquisition, Writing - original draft, Writing - review & editing. **Mao Mao:** Writing - original draft. **Hui Zhu:** Writing - original draft. **Hu Cai:** Funding acquisition. **Dichen Li:** Funding acquisition, Supervision. **Jiankang He:** Conceptualization, Funding acquisition, Supervision, Writing - original draft, Writing - review & editing.

Declaration of competing interest

The authors declare that they have no known competing financial interests or personal relationships that could have appeared to influence the work reported in this paper.

Data availability

No data was used for the research described in the article.

Acknowledgments

This work was financially supported by the National Key Research and Development Program of China (2018YFA0703003), the National Natural Science Foundation of China (52125501), the Key Research Project of Shaanxi Province (2021LLRH-08), the Guangdong Basic and Applied Basic Research Foundation (2020B1515130002), the Research and Development Project of Shaanxi Province (2023-ZDLSF-08), the Program for Innovation Team of Shaanxi Province (2023-CX-TD-17) and the Fundamental Research Funds for the Central Universities.

Abbreviations

CVD, cardiovascular disease; CM, cardiomyocyte; Cx43, connexin 43; Corrected action potential duration (cAPD); HiPSC, human induced pluripotent stem cells; HiPSC-CM, human induced pluripotent stem cells-derived cardiomyocyte; NRVM, neonatal rat ventricular myocyte; NHCF, normal human cardiac fibroblasts; HASC, human adipose-derived stem/stromal cell; HUVEC, human umbilical vein endothelial cell; HMVEC, human cardiac microvascular endothelial cell; ECM, extracellular matrix; EC, endothelial cell; PMMA, poly (methyl-methacrylate); PDMS, poly (dimethylsiloxane); PEGDA, poly (ethylene glycol) diacrylate; PCL, polycaprolactone; PICO, poly (itaconate-*co*-citrate-*co*-octanediol); GelMA, methacrylated gelatin; PLA, poly lactic acid; PANI, polyaniline; aOBB, anisotropic organ building block; μCOP, microscale continuous optical printing; SL, stereolithography; MJM, multi-jet modeling, FDM, fused deposition modeling; UCG, ultrasound cardiogram; SEM, scanning electron microscope; SNR, signal-to-noise ratio; MEMS, microelectromechanical system; ZnO, zinc oxide; IrOx, iridium oxide; NEA, nano-crown electrode array; MEA, micro-electrode array; MPS, microphysiological systems; FIB, focused ion-beam; Fast-inactivating potassium current, $I_{K(f)}$; Rapidly activating delayed rectifier current I_{Kr}; Inhibition constant, K_i; Dissociation constant, K_d; Half maximal inhibitory concentration, IC_{50}; Concentration for 50 % of maximal effect, EC_{50}.

References

[1] F. Zhang, K.-Y. Qu, B. Zhou, Y. Luo, Z. Zhu, D.-J. Pan, C. Cui, Y. Zhu, M.-L. Chen, N.-P. Huang, Design and fabrication of an integrated heart-on-a-chip platform for construction of cardiac tissue from human iPSC-derived cardiomyocytes and in situ evaluation of physiological function, Biosens. Bioelectron. 179 (2021).

[2] Y.S. Zhang, J. Aleman, A. Arneri, S. Bersini, F. Piraino, S.R. Shin, M.R. Dokmeci, A. Khademhosseini, From cardiac tissue engineering to heart-on-a-chip: beating challenges, Biomed. Mater. 10 (3) (2015).

[3] J. Sheng, Q. Li, T. Liu, X. Wang, Cerebrospinal fluid dynamics along the optic nerve, Front. Neurol. 13 (2022).

[4] C.W. Tsao, A.W. Aday, Z.I. Almarzooq, A. Alonso, A.Z. Beaton, M.S. Bittencourt, A.K. Boehme, A.E. Buxton, A.P. Carson, Y. Commodore-Mensah, M.S.V. Elkind, K. R. Evenson, C. Eze-Nliam, J.F. Ferguson, G. Generoso, J.E. Ho, R. Kalani, S. S. Khan, B.M. Kissela, K.L. Knutson, D.A. Levine, T.T. Lewis, J. Liu, M.S. Loop, J. Ma, M.E. Mussolino, S.D. Navaneethan, A.M. Perak, R. Poudel, M. Rezk-Hanna, G.A. Roth, E.B. Schroeder, S.H. Shah, E.L. Thacker, L.B. VanWagner, S.S. Virani, J.H. Voecks, N.-Y. Wang, K. Yaffe, S.S. Martin, E. Amer heart assoc council, S. Stroke stat, heart disease and stroke statistics-2022 update: a report from the American heart association, Circulation 145 (8) (2022) E153–E639.

[5] M. Yadid, H. Oved, E. Silberman, T. Dvir, Bioengineering approaches to treat the failing heart: from cell biology to 3D printing, Nat. Rev. Cardiol. 19 (2) (2022) 83–99.

[6] Y. Zhao, N. Rafatian, N.T. Feric, B.J. Cox, R. Aschar-Sobbi, E.Y. Wang, P. Aggarwal, B. Zhang, G. Conant, K. Ronaldson-Bouchard, A. Pahnke, S. Protze, J.H. Lee, L.D. Huyer, D. Jekic, A. Wickeler, H.E. Naguib, G.M. Keller, G. Vunjak-Novakovic, U. Broeckel, P.H. Backx, M. Radisic, A platform for generation of chamber-specific cardiac tissues and disease modeling, Cell 176 (4) (2019) 913–927.

[7] Y. Morimoto, S. Mori, S. Takeuchi, Ieee, 3D human cardiac muscle on A CHIP: quantification of contractile force of human IPS-derived cardiomyocytes, 28th IEEE Int. Conf. Micro Electro Mech. Syst. (MEMS), Estoril, PORTUGAL (2015) 566–568.

[8] Y. Morimoto, S. Mori, F. Sakai, S. Takeuchi, Human induced pluripotent stem cell-derived fiber-shaped cardiac tissue on a chip, Lab Chip 16 (12) (2016) 2295–2301.

[9] Y.S. Zhang, A. Arneri, S. Bersini, S.-R. Shin, K. Zhu, Z. Goli-Malekabadi, J. Aleman, C. Colosi, F. Busignani, V. Dell'Erba, C. Bishop, T. Shupe, D. Demarchi, M. Moretti, M. Rasponi, M.R. Dokmeci, A. Atala, A. Khademhosseini, Bioprinting 3D microfibrous scaffolds for engineering endothelialized myocardium and heart-on-a-chip, Biomaterials 110 (2016) 45–59.

[10] A. Arslan-Yildiz, R. El Assal, P. Chen, S. Guven, F. Inci, U. Demirci, Towards artificial tissue models: past, present, and future of 3D bioprinting, Biofabrication 8 (1) (2016).

[11] N. Noor, A. Shapira, R. Edri, I. Gal, L. Wertheim, T. Dvir, 3D printing of personalized thick and perfusable cardiac patches and hearts, Adv. Sci. 6 (11) (2019).

[12] M. Dey, I.T. Ozbolat, 3D bioprinting of cells, tissues and organs, Sci. Rep. 10 (1) (2020).

[13] M.A. Chliara, S. Elezoglou, I. Zergioti, Bioprinting on organ-on-chip: development and applications, Biosens. Bioelectron. 12 (12) (2022).

[14] Z. Qiu, H. Zhu, Y. Wang, A. Kasimu, D. Li, J. He, Functionalized alginate-based bioinks for microscale electrohydrodynamic bioprinting of living tissue constructs with improved cellular spreading and alignment, Bio-Design Manuf. 6 (2) (2023) 136–149.

[15] J. He, B. Zhang, Z. Li, M. Mao, J. Li, K. Han, D. Li, High-resolution electrohydrodynamic bioprinting: a new biofabrication strategy for biomimetic micro/nanoscale architectures and living tissue constructs, Biofabrication 12 (4) (2020).

[16] Q. Ma, H. Ma, F. Xu, X. Wang, W. Sun, Microfluidics in cardiovascular disease research: state of the art and future outlook, Microsyst. & Nanoeng. 7 (1) (2021).

[17] B. Zhang, A. Korolj, B.F.L. Lai, M. Radisic, Advances in organ-on-a-chip engineering, Nat. Rev. Mater. 3 (8) (2018) 257–278.

[18] S.N. Bhatia, D.E. Ingber, Microfluidic organs-on-chips, Nat. Biotechnol. 32 (8) (2014) 760–772.

[19] Y.S. Zhang, J. Aleman, S.R. Shin, T. Kilic, D. Kim, S.A.M. Shaegh, S. Massa, R. Riahi, S. Chae, N. Hu, H. Avci, W. Zhang, A. Silvestri, A.S. Nezhad, A. Manbohi, F. De Ferrari, A. Polini, G. Calzone, N. Shaikh, P. Alerasool, E. Budina, J. Kang, N. Bhise, J. Ribas, A. Pourmand, A. Skardal, T. Shupe, C.E. Bishop, M.R. Dokmeci, A. Atala, A. Khademhosseini, Multisensor-integrated organs-on-chips platform for automated and continual in situ monitoring of organoid behaviors, Proc. Natl. Acad. Sci. U.S.A. 114 (12) (2017) E2293–E2302.

[20] N.S. Bhise, J. Ribas, V. Manoharan, Y.S. Zhang, A. Polini, S. Massa, M.R. Dokmeci, A. Khademhosseini, Organ-on-a-chip platforms for studying drug delivery systems, J. Contr. Release 190 (2014) 82–93.

[21] F. Qian, C. Huang, Y.-D. Lin, A.N. Ivanovskaya, T.J. O'Hara, R.H. Booth, C. J. Creek, H.A. Enright, D.A. Soscia, A.M. Belle, R. Liao, F.C. Lightstone, K.S. Kulp, E.K. Wheeler, Simultaneous electrical recording of cardiac electrophysiology and contraction on chip, Lab Chip 17 (10) (2017) 1732–1739.

[22] L.A. MacQueen, S.P. Sheehy, C.O. Chantre, J.F. Zimmerman, F.S. Pasqualini, X. Liu, J.A. Goss, P.H. Campbell, G.M. Gonzalez, S.J. Park, A.K. Capulli, J. P. Ferrier, T.F. Kosar, L. Mahadevan, W.T. Pu, K.K. Parker, A tissue-engineered scale model of the heart ventricle, Nat. Biomed. Eng. 2 (12) (2018) 930–941.

[23] A.C. van Spreeuwel, N.A. Bax, A.J. Bastiaens, J. Foolen, S. Loerakker, M. Borochin, D.W. van der Schaft, C.S. Chen, F.P. Baaijens, C.V. Bouten, The influence of matrix (an)isotropy on cardiomyocyte contraction in engineered cardiac microtissues, Integr. Biol. 6 (4) (2014) 422–429.

[24] H. Liu, O.A. Bolonduro, N. Hu, J. Ju, A.A. Rao, B.M. Duffy, Z. Huang, L.D. Black, B.P. Timko, Heart-on-a-Chip model with integrated extra- and intracellular bioelectronics for monitoring cardiac electrophysiology under acute hypoxia, Nano Lett. 20 (4) (2020) 2585–2593.

[25] C. Xie, Z. Lin, L. Hanson, Y. Cui, B. Cui, Intracellular recording of action potentials by nanopillar electroporation, Nat. Nanotechnol. 7 (3) (2012) 185–190.
[26] M. Hofer, M.P. Lutolf, Engineering organoids, Nat. Rev. Mater. 6 (5) (2021) 402–420.
[27] J. Criscione, Z. Rezaei, C.M.H. Cantu, S. Murphy, S.R. Shin, D.-H. Kim, Heart-on-a-chip platforms and biosensor integration for disease modeling and phenotypic drug screening, Biosens. Bioelectron. 220 (2023).
[28] K.W. Cho, W.H. Lee, B.-S. Kim, D.-H. Kim, Sensors in heart-on-a-chip: a review on recent progress, Talanta 219 (2020).
[29] X. Li, H. Zhu, B. Gu, C. Yao, Y. Gu, W. Xu, J. Zhang, J. He, X. Liu, D. Li, Advancing Intelligent Organs-On-A-Chip Systems with Comprehensive in Situ Bioanalysis, Advanced Materials, Deerfield Beach, Fla., 2023, e2305268-e2305268.
[30] X. Li, M. Mao, K. Han, C. Yao, B. Gu, J. He, D. Li, 3D conductive material strategies for modulating and monitoring cells, Prog. Mater. Sci. 133 (2023).
[31] J. Liu, K. Miller, X. Ma, S. Dewan, N. Lawrence, G. Whang, P. Chung, A. D. McCulloch, S. Chen, Direct 3D bioprinting of cardiac micro-tissues mimicking native myocardium, Biomaterials (2020) 256.
[32] B. Gu, X. Li, C. Yao, X. Qu, M. Mao, D. Li, J. He, Integration of microelectrodes and highly-aligned cardiac constructs for in situ electrophysiological recording, Microchem. J. 190 (2023).
[33] C. O'Connor, E. Brady, Y. Zheng, E. Moore, K.R. Stevens, Engineering the multiscale complexity of vascular networks, Nat. Rev. Mater. 7 (9) (2022) 702–716.
[34] M. Abulaiti, Y. Yalikun, K. Murata, A. Sato, M.M. Sami, Y. Sasaki, Y. Fujiwara, K. Minatoya, Y. Shiba, Y. Tanaka, H. Masumoto, Establishment of a heart-on-a-chip microdevice based on human iPS cells for the evaluation of human heart tissue function, Sci. Rep. 10 (1) (2020).
[35] K. Han, J. He, L. Fu, M. Mao, Y. Kang, D. Li, Engineering highly-aligned three-dimensional (3D) cardiac constructs for enhanced myocardial infarction repair, Biofabrication 15 (1) (2023).
[36] T. Anada, J. Fukuda, Y. Sai, O. Suzuki, An oxygen-permeable spheroid culture system for the prevention of central hypoxia and necrosis of spheroids, Biomaterials 33 (33) (2012) 8430–8441.
[37] N. Annabi, K. Tsang, S.M. Mithieux, M. Nikkhah, A. Ameri, A. Khademhosseini, A. S. Weiss, Highly elastic micropatterned hydrogel for engineering functional cardiac tissue, Adv. Funct. Mater. 23 (39) (2013) 4950–4959.
[38] S.P. Sheehy, A. Grosberg, P. Qin, D.J. Behm, J.P. Ferrier, M.A. Eagleson, A. P. Nesmith, D. Krull, J.G. Falls, P.H. Campbell, M.L. McCain, R.N. Willette, E. Hu, K.K. Parker, Toward improved myocardial maturity in an organ-on-chip platform with immature cardiac myocytes, Exp. Biol. Med. 242 (17) (2017) 1643–1656.
[39] A. Alassaf, G. Tansik, V. Mayo, L. Wubker, D. Carbonero, A. Agarwal, Engineering anisotropic cardiac monolayers on microelectrode arrays for non-invasive analyses of electrophysiological properties, Analyst 145 (1) (2020) 139–149.
[40] P. Camelliti, J.O. Gallagher, P. Kohl, A.D. McCulloch, Micropatterned cell cultures on elastic membranes as an in vitro model of myocardium, Nat. Protoc. 1 (3) (2006) 1379–1391.
[41] E. Cimetta, S. Pizzato, S. Bollini, E. Serena, P. De Coppi, N. Elvassore, Production of arrays of cardiac and skeletal muscle myofibers by micropatterning techniques on a soft substrate, Biomed. Microdevices 11 (2) (2009) 389–400.
[42] J.U. Lind, T.A. Busbee, A.D. Valentine, F.S. Pasqualini, H. Yuan, M. Yadid, S.-J. Park, A. Kotikian, A.P. Nesmith, P.H. Campbell, J.J. Vlassak, J.A. Lewis, K. K. Parker, Instrumented cardiac microphysiological devices via multimaterial three-dimensional printing, Nat. Mater. 16 (3) (2017) 303–308.
[43] A.G. Kleber, Y. Rudy, Basic mechanisms of cardiac impulse propagation and associated arrhythmias, Physiol. Rev. 84 (2) (2004) 431–488.
[44] Y. Morimoto, S. Mori, F. Sakai, S. Takeuchi, Human induced pluripotent stem cell-derived fiber-shaped cardiac tissue on a chip, Lab Chip 16 (12) (2016) 2295–2301.
[45] I.C. Turnbull, I. Karakikes, G.W. Serrao, P. Backeris, J.J. Lee, C. Xie, G. Senyei, R. E. Gordon, R.A. Li, F.G. Akar, R.J. Hajjar, J.S. Hulot, K.D. Costa, Advancing functional engineered cardiac tissues toward a preclinical model of human myocardium, Faseb. J. 28 (2) (2014) 644–654.
[46] T. Boudou, W.R. Legant, A. Mu, M.A. Borochin, N. Thavandiran, M. Radisic, P. W. Zandstra, J.A. Epstein, K.B. Margulies, C.S. Chen, A microfabricated platform to measure and manipulate the mechanics of engineered cardiac microtissues, Tissue Eng Part A 18 (9–10) (2012) 910–919.
[47] B. Liau, N. Christoforou, K.W. Leong, N. Bursac, Pluripotent stem cell-derived cardiac tissue patch with advanced structure and function, Biomaterials 32 (35) (2011) 9180–9187.
[48] L.D. Black III, J.D. Meyers, J.S. Weinbaum, Y.A. Shvelidze, R.T. Tranquillo, Cell-induced alignment augments twitch force in fibrin gel-based engineered myocardium via gap junction modification, Tissue Eng. 15 (10) (2009) 3099–3108.
[49] W. Bian, N. Badie, H.D. Himel, N. Bursac, Robust T-tubulation and maturation of cardiomyocytes using tissue engineered epicardial mimetics, Biomaterials 35 (12) (2014) 3819–3828.
[50] W. Bian, B. Liau, N. Badie, N. Bursac, Mesoscopic hydrogel molding to control the 3D geometry of bioartificial muscle tissues, Nat. Protoc. 4 (10) (2009) 1522–1534.
[51] M. Mao, J. He, Z. Li, K. Han, D. Li, Multi-directional cellular alignment in 3D guided by electrohydrodynamically-printed microlattices, Acta Biomater. 101 (2020) 141–151.
[52] D. Rosenfeld, S. Landau, Y. Shandalov, N. Raindel, A. Freiman, E. Shor, Y. Blinder, H.H. Vandenburgh, D.J. Mooney, S. Levenberg, Morphogenesis of 3D vascular networks is regulated by tensile forces, Proc. Natl. Acad. Sci. U.S.A. 113 (12) (2016) 3215–3220.
[53] J.S. Miller, K.R. Stevens, M.T. Yang, B.M. Baker, D.-H.T. Nguyen, D.M. Cohen, E. Toro, A.A. Chen, P.A. Galie, X. Yu, R. Chaturvedi, S.N. Bhatia, C.S. Chen, Rapid casting of patterned vascular networks for perfusable engineered three-dimensional tissues, Nat. Mater. 11 (9) (2012) 768–774.
[54] D.B. Kolesky, K.A. Homan, M.A. Skylar-Scott, J.A. Lewis, Three-dimensional bioprinting of thick vascularized tissues, Proc. Natl. Acad. Sci. U.S.A. 113 (12) (2016) 3179–3184.
[55] S. Kusuma, Y.-I. Shen, D. Hanjaya-Putra, P. Mali, L. Cheng, S. Gerecht, Self-organized vascular networks from human pluripotent stem cells in a synthetic matrix, Proc. Natl. Acad. Sci. U.S.A. 110 (31) (2013) 12601–12606.
[56] Y. Tsukamoto, T. Akagi, M. Akashi, Vascularized cardiac tissue construction with orientation by layer-by-layer method and 3D printer, Sci. Rep. 10 (1) (2020).
[57] J. Morrissette-McAlmon, B. Ginn, S. Somers, T. Fukunishi, C. Thanitcul, A. Rindone, N. Hibino, L. Tung, H.-Q. Mao, W. Grayson, Biomimetic model of contractile cardiac tissue with endothelial networks stabilized by adipose-derived stromal/stem cells, Sci. Rep. 10 (1) (2020).
[58] M.A. Skylar-Scott, S.G.M. Uzel, L.L. Nam, J.H. Ahrens, R.L. Truby, S. Damaraju, J. A. Lewis, Biomanufacturing of organ-specific tissues with high cellular density and embedded vascular channels, Sci. Adv. 5 (9) (2019).
[59] F. Maiullari, M. Costantini, M. Milan, V. Pace, M. Chirivi, S. Maiullari, A. Rainer, D. Baci, H.E.-S. Marei, D. Seliktar, C. Gargioli, C. Bearzi, R. Rizzi, A multi-cellular 3D bioprinting approach for vascularized heart tissue engineering based on HUVECs and iPSC-derived cardiomyocytes, Sci. Rep. 8 (2018).
[60] C. Colosi, S.R. Shin, V. Manoharan, S. Massa, M. Costantini, A. Barbetta, M. R. Dokmeci, M. Dentini, A. Khademhosseini, Microfl uidic bioprinting of heterogeneous 3D tissue constructs using low-viscosity bioink, Adv. Mater. 28 (4) (2016) 677–684.
[61] W.L. Stoppel, D.L. Kaplan, L.D. Black III, Electrical and mechanical stimulation of cardiac cells and tissue constructs, Adv. Drug Deliv. Rev. 96 (2016) 135–155.
[62] K. Ronaldson-Bouchard, K. Yeager, D. Teles, T. Chen, S. Ma, L. Song, K. Morikawa, H.M. Wobma, A. Vasciaveo, E.C. Ruiz, M. Yazawa, G. Vunjak-Novakovic, Engineering of human cardiac muscle electromechanically matured to an adult-like phenotype, Nat. Protoc. 14 (10) (2019) 2781–2817.
[63] M. Carlos-Oliveira, F. Lozano-Juan, P. Occhetta, R. Visone, M. Rasponi, Current strategies of mechanical stimulation for maturation of cardiac microtissues, Biophys. Rev. 13 (5) (2021) 717–727.
[64] J.J. Tomasek, E.D. Hay, Analysis of the role of microfilaments and microtubules in acquisition of bipolarity and elongation of fibroblasts in hydrated collagen gels, JCB (J. Cell Biol.) 99 (2) (1984) 536–549.
[65] C. Tamiello, A.B.C. Buskermolen, F.P.T. Baaijens, J.L.V. Broers, C.V.C. Bouten, Heading in the right direction: understanding cellular orientation responses to complex biophysical environments, Cell. Mol. Bioeng. 9 (1) (2016) 12–37.
[66] B.D. Hoffman, C. Grashoff, M.A. Schwartz, Dynamic molecular processes mediate cellular mechanotransduction, Nature 475 (7356) (2011) 316–323.
[67] I.L. Chin, L. Hool, Y.S. Choi, Interrogating cardiac muscle cell mechanobiology on stiffness gradient hydrogels, Biomater. Sci. 9 (20) (2021) 6795–6806.
[68] B. Bhana, R.K. Iyer, W.L.K. Chen, R. Zhao, K.L. Sider, M. Likhitpanichkul, C. A. Simmons, M. Radisic, Influence of substrate stiffness on the phenotype of heart cells, Biotechnol. Bioeng. 105 (6) (2010) 1148–1160.
[69] J.M. Bliley, M.C.S.C. Vermeer, R.M. Duffy, I. Batalov, D. Kramer, J.W. Tashman, D.J. Shiwarski, A. Lee, A.S. Teplenin, L. Volkers, B. Coffin, M.F. Hoes, A. Kalmykov, R.N. Palchesko, Y. Sun, J.D.H. Jongbloed, N. Bomer, R.A. de Boer, A.J.H. Suurmeijer, D.A. Pijnappels, M.C. Bolling, P. van der Meer, A.W. Feinberg, Dynamic loading of human engineered heart tissue enhances contractile function and drives a desmosome-linked disease phenotype, Sci. Transl. Med. 13 (603) (2021).
[70] C.P. Jackman, A.L. Carlson, N. Bursac, Dynamic culture yields engineered myocardium with near-adult functional output, Biomaterials 111 (2016) 66–79.
[71] M. Lux, B. Andree, T. Horvath, A. Nosko, D. Manikowski, D. Hilfiker-Kleiner, A. Haverich, A. Hilfiker, In vitro maturation of large-scale cardiac patches based on a perfusable starter matrix by cyclic mechanical stimulation, Acta Biomater. 30 (2016) 177–187.
[72] C.-W. Hsiao, M.-Y. Bai, Y. Chang, M.-F. Chung, T.-Y. Lee, C.-T. Wu, B. Maiti, Z.-X. Liao, R.-K. Li, H.-W. Sung, Electrical coupling of isolated cardiomyocyte clusters grown on aligned conductive nanofibrous meshes for their synchronized beating, Biomaterials 34 (4) (2013) 1063–1072.
[73] Y. Li, L. Wei, L. Lan, Y. Gao, Q. Zhang, H. Dawit, J. Mao, L. Guo, L. Shen, L. Wang, Conductive biomaterials for cardiac repair: a review, Acta Biomater. 139 (2022) 157–178.
[74] L. Wang, Y. Wu, T. Hu, B. Guo, P.X. Ma, Electrospun conductive nanofibrous scaffolds for engineering cardiac tissue and 3D bioactuators, Acta Biomater. 59 (2017) 68–81.
[75] K. Roshanbinfar, L. Vogt, B. Greber, S. Diecke, A.R. Boccaccini, T. Scheibel, F. B. Engel, Electroconductive biohybrid hydrogel for enhanced maturation and beating properties of engineered cardiac tissues, Adv. Funct. Mater. 28 (42) (2018).
[76] G. Eng, B.W. Lee, L. Protas, M. Gagliardi, K. Brown, R.S. Kass, G. Keller, R. B. Robinson, G. Vunjak-Novakovic, Autonomous beating rate adaptation in human stem cell-derived cardiomyocytes, Nat. Commun. 7 (2016).
[77] A. Adan, Y. Kiraz, Y. Baran, Cell proliferation and cytotoxicity assays, Curr. Pharmaceut. Biotechnol. 17 (14) (2016) 1213–1221.
[78] K.F. Goliwas, J.R. Richter, H.C. Pruitt, L.M. Araysi, N.R. Anderson, R.S. Samant, S. M. Lobo-Ruppert, J.L. Berry, A.R. Frost, Methods to evaluate cell growth, viability, and response to treatment in a tissue engineered breast cancer model, Sci. Rep. 7 (2017).

[79] R.A. Gray, D.N. Mashburn, V.Y. Sidorov, J.P. Wikswo, Quantification of transmembrane currents during action potential propagation in the heart, Biophys. J. 104 (1) (2013) 268–278.
[80] J.M. Rhett, J. Jourdan, R.G. Gourdie, Connexin 43 connexon to gap junction transition is regulated by zonula occludens-1, Mol. Biol. Cell 22 (9) (2011) 1516–1528.
[81] M.M. Slotvitsky, V.A. Tsvelaya, A.D. Podgurskaya, K.I. Agladze, Formation of an electrical coupling between differentiating cardiomyocytes, Sci. Rep. 10 (1) (2020).
[82] W. Dou, M. Malhi, Q. Zhao, L. Wang, Z. Huang, J. Law, N. Liu, C.A. Simmons, J. T. Maynes, Y. Sun, Microengineered platforms for characterizing the contractile function of in vitro cardiac models, Microsyst. & Nanoeng. 8 (1) (2022).
[83] A.O. Grant, Cardiac ion channels, Circulation-Arrhythmia and Electrophysiol. 2 (2) (2009) 185–194.
[84] S. Alonso, M. Baer, B. Echebarria, Nonlinear physics of electrical wave propagation in the heart: a review, Rep. Prog. Phys. 79 (9) (2016).
[85] R. Hugang, L. Zhongchi, S. Elinav, P. Yingtian, R. Fine, D. Congwu, Simultaneous Assessing The Intracellular Potassium And Calcium Concentrations Noninvasively In Vivo With High Resolution Fluorescence Imaging. 2011 8th International Conference & Expo on Emerging Technologies for a Smarter World, 2011, p. 6.
[86] A. Bullen, P. Saggau, Indicators and optical configuration for simultaneous high-resolution recording of membrane potential and intracellular calcium using laser scanning microscopy, Pflueg. Arch. Eur. J. Physiol. 436 (5) (1998) 788–796.
[87] V.G. Fast, Simultaneous optical imaging of membrane potential and intracellular calcium, J. Electrocardiol. 38 (4) (2005) 107–112.
[88] Y.-J. Chen, Y.-C. Chen, S.-A. Chen, C.-I. Lin, Cardiac cellular electrophysiology, voltage clamp, and patch clamp, Acta Cardiol. Sin. 25 (2) (2009) 59–63.
[89] M. Bebarova, Advances in patch clamp technique: towards higher quality and quantity, Gen. Physiol. Biophys. 31 (2) (2012) 131–140.
[90] Y. Liang, M. Ernst, F. Brings, D. Kireev, V. Maybeck, A. Offenhaeusser, D. Mayer, High performance flexible organic electrochemical transistors for monitoring cardiac action potential, Adv. Healthcare Mater. 7 (19) (2018).
[91] A. Kalmykov, C. Huang, J. Bliley, D. Shiwarski, J. Tashman, A. Abdullah, S. K. Rastogi, S. Shukla, E. Mataev, A.W. Feinberg, K.J. Hsia, T. Cohen-Karni, Organ-on-e-chip: three-dimensional self-rolled biosensor array for electrical interrogations of human electrogenic spheroids, Sci. Adv. 5 (8) (2019).
[92] B. Gu, X. Li, C. Yao, X. Qu, M. Mao, D. Li, J. He, Integration of microelectrodes and highly-aligned cardiac constructs for in situ electrophysiological recording, Microchem. J. 190 (2023).
[93] X. Dai, W. Zhou, T. Gao, J. Liu, C.M. Lieber, Three-dimensional mapping and regulation of action potential propagation in nanoelectronics-innervated tissues, Nat. Nanotechnol. 11 (9) (2016) 776–782.
[94] Q. Li, K. Nan, P. Le Floch, Z. Lin, H. Sheng, T.S. Blum, J. Liu, Cyborg organoids: implantation of nanoelectronics via organogenesis for tissue-wide electrophysiology, Nano Lett. 19 (8) (2019) 5781–5789.
[95] M.E. Spira, A. Hai, Multi-electrode array technologies for neuroscience and cardiology, Nat. Nanotechnol. 8 (2) (2013) 83–94.
[96] I. Suzuki, M. Fukuda, K. Shirakawa, H. Jiko, M. Gotoh, Carbon nanotube multi-electrode array chips for noninvasive real-time measurement of dopamine, action potentials, and postsynaptic potentials, Biosens. Bioelectron. 49 (2013) 270–275.
[97] H.-f. Chen, K. Gao, S. Qi, X. Zhu, A planar multielectrode array with microfluidics channel, International Symposium on Biomedicine and Engineering (ISBE 2011), Bali Island, INDONESIA (2011) 132–136.
[98] N. Hu, D. Xu, J. Fang, H. Li, J. Mo, M. Zhou, B. Li, H.-j. Chen, T. Zhang, J. Feng, T. Hang, W. Xia, X. Chen, X. Liu, G. He, X. Xie, Intracellular recording of cardiomyocyte action potentials by nanobranched microelectrode array, Biosens. Bioelectron. 169 (2020).
[99] A. Hai, J. Shappir, M.E. Spira, In-cell recordings by extracellular microelectrodes, Nat. Methods 7 (3) (2010) 200–202.
[100] C. Xie, Z. Lin, L. Hanson, Y. Cui, B. Cui, Intracellular recording of action potentials by nanopillar electroporation, Nat. Nanotechnol. 7 (3) (2012) 185–190.
[101] Z.C. Lin, C. Xie, Y. Osakada, Y. Cui, B. Cui, Iridium oxide nanotube electrodes for sensitive and prolonged intracellular measurement of action potentials, Nat. Commun. 5 (2014).
[102] B.X.E. Desbiolles, E. de Coulon, A. Bertsch, S. Rohr, P. Renaud, Intracellular recording of cardiomyocyte action potentials with nanopatterned volcano-shaped microelectrode arrays, Nano Lett. 19 (9) (2019) 6173–6181.
[103] Z. Jahed, Y. Yang, C.-T. Tsai, E.P. Foster, A.F. McGuire, H. Yang, A. Liu, C. Forro, Z. Yan, X. Jiang, M.-T. Zhao, W. Zhang, X. Li, T. Li, A. Pawlosky, J.C. Wu, B. Cui, Nanocrown electrodes for parallel and robust intracellular recording of cardiomyocytes, Nat. Commun. 13 (1) (2022).
[104] Y. Yang, A. Liu, C.T. Tsai, C. Liu, J.C. Wu, B. Cui, Cardiotoxicity drug screening based on whole-panel intracellular recording, Biosens. Bioelectron. 216 (2022).
[105] A. Salameh, A. Wustmann, S. Karl, K. Blanke, D. Apel, D. Rojas-Gomez, H. Franke, F.W. Mohr, J. Janousek, S. Dhein, Cyclic mechanical stretch induces cardiomyocyte orientation and polarization of the gap junction protein Connexin43, Circ. Res. 106 (10) (2010) 1592–1602.
[106] X. Trepat, L. Deng, S.S. An, D. Navajas, D.J. Tschumperlin, W.T. Gerthoffer, J. P. Butler, J.J. Fredberg, Universal physical responses to stretch in the living cell, Nature 447 (7144) (2007) 592–595.
[107] D. Kabanov, S. Klimovic, V. Rotrekl, M. Pesl, J. Pribyl, Atomic force spectroscopy is a promising tool to study contractile properties of cardiac cells, Micron 155 (2022).
[108] E. Potter, T.H. Marwick, Assessment of left ventricular function by echocardiography the case for routinely adding global longitudinal strain to ejection fraction, Jacc-Cardiovasc. Imag. 11 (2) (2018) 260–274.
[109] X. Yang, M. Rodriguez, L. Pabon, K.A. Fischer, H. Reinecke, M. Regnier, N. J. Sniadecki, H. Ruohola-Baker, C.E. Murry, Tri-iodo-L-thyronine promotes the maturation of human cardiomyocytes-derived from induced pluripotent stem cells, J. Mol. Cell. Cardiol. 72 (2014) 296–304.
[110] K.M. Beussman, M.L. Rodriguez, A. Leonard, N. Taparia, C.R. Thompson, N. J. Sniadecki, Micropost arrays for measuring stem cell-derived cardiomyocyte contractility, Methods 94 (2016) 43–50.
[111] D.-S. Kim, Y.W. Choi, A. Shanmugasundaram, Y.-J. Jeong, J. Park, N.-E. Oyunbaatar, E.-S. Kim, M. Choi, D.-W. Lee, Highly durable crack sensor integrated with silicone rubber cantilever for measuring cardiac contractility, Nat. Commun. 11 (1) (2020).
[112] L.A. MacQueen, S.P. Sheehy, C.O. Chantre, J.F. Zimmerman, F.S. Pasqualini, X. Liu, J.A. Goss, P.H. Campbell, G.M. Gonzalez, S.-J. Park, A.K. Capulli, J. P. Ferrier, T.F. Kosarl, L. Mahadevan, W.T. Pu, K.K. Parker, A tissue-engineered scale model of the heart ventricle, Nat. Biomed. Eng. 2 (12) (2018) 930–941.
[113] N.-E. Oyunbaatar, A. Shanmugasundaram, D.-W. Lee, Contractile behaviors of cardiac muscle cells on mushroom-shaped micropillar arrays, Colloids Surf. B Biointerfaces 174 (2019) 103–109.
[114] K. Matsudaira, H. Takahashi, K. Hirayama-Shoji, T.-V. Nguyen, T. Tsukagoshi, I. Shimoyama, A MEMS-based measurement system for evaluating the force-length relationship of human induced pluripotent stem cell-derived cardiomyocytes adhered on a substrate, J. Micromech. Microeng. 29 (5) (2019).
[115] K. Matsudaira, N. Thanh-Vinh, K.H. Shoji, T. Tsukagoshi, T. Takahata, I. Shimoyama, MEMS piezoresistive cantilever for the direct measurement of cardiomyocyte contractile force, J. Micromech. Microeng. 27 (10) (2017).
[116] A.W. Feinberg, A. Feigel, S.S. Shevkoplyas, S. Sheehy, G.M. Whitesides, K. K. Parker, Muscular thin films for building actuators and powering devices, Science 317 (5843) (2007) 1366–1370.
[117] J. Park, J. Ryu, S.K. Choi, E. Seo, J.M. Cha, S. Ryu, J. Kim, B. Kim, S.H. Lee, Real-time measurement of the contractile forces of self-organized cardiomyocytes on hybrid biopolymer microcantilevers, Anal. Chem. 77 (20) (2005) 6571–6580.
[118] L. Sun, Z. Chen, D. Xu, Y. Zhao, Electroconductive and anisotropic structural color hydrogels for visual heart-on-a-chip construction, Adv. Sci. 9 (16) (2022).
[119] M. Mullner, M.M. Hirschl, H. Herkner, F. Sterz, T. Leitha, M. Exner, M. Binder, A. N. Laggner, Creatine kinase-MB fraction and cardiac troponin T to diagnose acute myocardial infarction after cardiopulmonary resuscitation, J. Am. Coll. Cardiol. 28 (5) (1996) 1220–1225.
[120] P. Hong, W. Li, J. Li, Applications of aptasensors in clinical diagnostics, Sensors 12 (2) (2012) 1181–1193.
[121] S.R. Shin, Y.S. Zhang, D.-J. Kim, A. Manbohi, H. Avci, A. Silvestri, J. Aleman, N. Hu, T. Kilic, W. Keung, M. Righi, P. Assawes, H.A. Alhadrami, R.A. Li, M. R. Dokmeci, A. Khademhosseini, Aptamer-based microfluidic electrochemical biosensor for monitoring cell-secreted trace cardiac biomarkers, Anal. Chem. 88 (20) (2016) 10019–10027.
[122] J. Lee, S. Mehrotra, E. Zare-Eelanjegh, R.O. Rodrigues, A. Akbarinejad, D. Ge, L. Amato, K. Kiaee, Y. Fang, A. Rosenkranz, W. Keung, B.B. Mandal, R.A. Li, T. Zhang, H. Lee, M.R. Dokmeci, Y.S. Zhang, A. Khademhosseini, S.R. Shin, A heart-breast cancer-on-a-chip platform for disease modeling and monitoring of cardiotoxicity induced by cancer chemotherapy, Small 17 (15) (2021).
[123] M.S. Shah, M. Brownlee, Molecular and cellular mechanisms of cardiovascular disorders in diabetes, Circ. Res. 118 (11) (2016) 1808–1829.
[124] O. Mourad, R. Yee, M. Li, S.S.S. Nunes, Modeling heart diseases on a chip: advantages and future opportunities, Circ. Res. 132 (4) (2023) 483–497.
[125] A.P. Alivisatos, M. Chun, G.M. Church, K. Deisseroth, J.P. Donoghue, R. J. Greenspan, P.L. McEuen, M.L. Roukes, T.J. Sejnowski, P.S. Weiss, R. Yuste, The brain activity map, Science 339 (6125) (2013) 1284–1285.
[126] M. Weber, N. Scherf, A.M. Meyer, D. Panakova, P. Kohl, J. Huisken, Cell-accurate optical mapping across the entire developing heart, Elife 6 (2017).
[127] T.J. Kolanowski, M. Busek, M. Schubert, A. Dmitrieva, B. Binnewerg, J. Poeche, K. Fisher, F. Schmieder, S. Gruenzner, S. Hansen, A. Richter, A. El-Armouche, F. Sonntag, K. Guan, Enhanced structural maturation of human induced pluripotent stem cell-derived cardiomyocytes under a controlled microenvironment in a microfluidic system, Acta Biomater. 102 (2020) 273–286.
[128] O. Mourad, R. Yee, M. Li, S.S. Nunes, Modeling heart diseases on a chip: advantages and future opportunities, Circ. Res. 132 (4) (2023) 483–497.
[129] J.H. van Weerd, V.M. Christoffels, The formation and function of the cardiac conduction system, Development 143 (2) (2016) 197–210.
[130] K. Williams, T. Liang, S. Masse, S. Khan, R. Hatkar, G. Keller, K. Nanthakumar, S. S. Nunes, A 3-D human model of complex cardiac arrhythmias, Acta Biomater. 132 (2021) 149–161.
[131] T.M. Spencer, R.F. Blumenstein, K.M. Pryse, S.-L. Lee, D.A. Glaubke, B.E. Carlson, E.L. Elson, G.M. Genin, Fibroblasts slow conduction velocity in a reconstituted tissue model of fibrotic cardiomyopathy, ACS Biomater. Sci. Eng. 3 (11) (2017) 3022–3028.
[132] E.Y. Wang, N. Rafatian, Y. Zhao, A. Lee, B.F.L. Lai, R.X. Lu, D. Jekic, L.D. Huyer, E.J. Knee-Walden, S. Bhattacharya, P.H. Backx, M. Radisic, Biowire model of interstitial and focal cardiac fibrosis, ACS Cent. Sci. 5 (7) (2019) 1146–1158.
[133] R.A. Graham, D.P. Frazier, J.W. Thompson, S. Haliko, H.F. Li, B.J. Wasserlauf, M. G. Spiga, N.H. Bishopric, K.A. Webster, A unique pathway of cardiac myocyte death caused by hypoxia-acidosis, J. Exp. Biol. 207 (18) (2004) 3189–3200.
[134] M.A. Laflamme, C.E. Murry, Heart regeneration, Nature 473 (7347) (2011) 326–335.
[135] L. Ren, W. Liu, Y. Wang, J.-C. Wang, Q. Tu, J. Xu, R. Liu, S.-F. Shen, J. Wang, Investigation of hypoxia-induced myocardial injury dynamics in a tissue interface mimicking microfluidic device, Anal. Chem. 85 (1) (2013) 235–244.

[136] X. Li, L. Zhao, Z. Chen, Y. Lin, P. Yu, L. Mao, Continuous electrochemical monitoring of extracellular lactate production from neonatal rat cardiomyocytes following myocardial hypoxia, Anal. Chem. 84 (12) (2012) 5285–5291.
[137] H. Liu, O.A. Bolonduro, N. Hu, J. Ju, A.A. Rao, B.M. Duffy, Z. Huang, L.D. Black, B.P. Timko, Heart-on-a-Chip model with integrated extra- and intracellular bioelectronics for monitoring cardiac electrophysiology under acute hypoxia, Nano Lett. 20 (4) (2020) 2585–2593.
[138] S.J. Kehl, QUINIDINE-INDUCED inhibition of the fast transient outward K+ current in rat melanotrophs, Br. J. Pharmacol. 103 (3) (1991) 1807–1813.
[139] D.M. Roden, R.L. Woosley, CLASS-I antiarrhythmic agents - quinidine, procainamide and N-acetylprocainamide, DISOPYRAMIDE, Pharmacology & Therapeutics 23 (2) (1983) 179–191.
[140] C. Wolpert, R. Schimpf, C. Giustetto, C. Antzelevitch, J. Cordeiro, R. Dumaine, R. Brugada, K. Hong, U. Bauersfeld, F. Gaita, M. Borggrefe, Further insights into the effect of quinidine in short QT syndrome caused by a mutation in HERG, J. Cardiovasc. Electrophysiol. 16 (1) (2005) 54–58.
[141] M. Gwilt, R.C. King, A.A. Milne, A.M. Solca, DOFETILIDE, a new class-III antiarrhythmic agent, reduces pacing induced heterogeneity of repolarization INVIVO, Cardiovasc. Res. 26 (11) (1992) 1102–1108.
[142] B.P. Bean, C.J. Cohen, R.W. Tsien, Lidocaine block of cardiac sodium-channels, J. Gen. Physiol. 81 (5) (1983) 613–642.
[143] T.R. Cummins, Setting up for the block: the mechanism underlying lidocaine's use-dependent inhibition of sodium channels, J. Physiol.-London 582 (1) (2007) 11, 11.
[144] H. Watanabe, N. Chopra, D. Laver, H.S. Hwang, S.S. Davies, D.E. Roach, H.J. Duff, D.M. Roden, A.A.M. Wilde, B.C. Knollmann, Flecainide prevents catecholaminergic polymorphic ventricular tachycardia in mice and humans, Nat. Med. 15 (4) (2009) 380–383.
[145] E. Aliot, A. Capucci, H.J. Crijns, A. Goette, J. Tamargo, Twenty-five years in the making: flecainide is safe and effective for the management of atrial fibrillation, Europace 13 (2) (2011) 161–173.
[146] L. Wang, X. Xu, J. Chen, W. Su, F. Zhang, A. Li, C. Li, C. Xu, Y. Sun, Crack sensing of cardiomyocyte contractility with high sensitivity and stability, ACS Nano. 16 (8) (2022) 12645–12655.
[147] M.E. Conolly, D.S. Davies, M. Sandler, C.D. Morgan, C.T. Dollery, J.W. Paterson, Metabolism of isoprenaline in dog and man, Br. J. Pharmacol. 46 (3) (1972) 458–&.
[148] I. Ostadalova, F. Kolar, B. Ostadal, V. Rohlicek, J. Rohlicek, J. Prochazka, Early postnatal-development of contractile performance and responsiveness to CA2+, verapamil and ryanodine in the isolated rat-heart, J. Mol. Cell. Cardiol. 25 (6) (1993) 733–740.
[149] P. Sermsappasuk, O. Abdelrahman, M. Weiss, Modeling cardiac uptake and negative inotropic response of verapamil in rat heart: effect of amiodarone, Pharmaceut. Res. 24 (1) (2007) 48–57.
[150] H. Sacks, B.M. Kennelly, Verapamil in cardiac-arrhythmias, Br. Med. J. 2 (5815) (1972) 716–&.
[151] S. Galandrin, M. Bouvier, Distinct signaling profiles of β_1 and β_2 adrenergic receptor ligands toward adenylyl cyclase and mitogen-activated protein kinase reveals the pluridimensionality of efficacy, Mol. Pharmacol. 70 (5) (2006) 1575–1584.
[152] B.P. Ramos, A.F.T. Arnsten, Adrenergic pharmacology and cognition: focus on the prefrontal cortex, Pharmacol. Therapeut. 113 (3) (2007) 523–536.
[153] D.J. Conklin, P. Haberzettl, G. Jagatheesan, S. Baba, M.L. Merchant, R.A. Prough, J.D. Williams, S.D. Prabhu, A. Bhatnagar, Glutathione *S*-transferase P protects against cyclophosphamide-induced cardiotoxicity in mice, Toxicol. Appl. Pharmacol. 285 (2) (2015) 136–148.
[154] C. Oleaga, A. Riu, S. Rothemund, A. Lavado, C.W. McAleer, C.J. Long, K. Persaud, N.S. Narasimhan, T. My, J. Roles, C.A. Carmona-Moran, T. Sasserath, D. H. Elbrecht, L. Kumanchik, L.R. Bridges, C. Martin, M.T. Schnepper, G. Ekman, M. Jackson, Y.I. Wang, R. Note, J. Langer, S. Teissier, J.J. Hickman, Investigation of the effect of hepatic metabolism on off-target cardiotoxicity in a multi-organ human-on-a-chip system, Biomaterials 182 (2018) 176–190.
[155] M. Didagelos, A. Boutis, N. Diamantopoulos, M. Sotiriadou, C. Fotiou, Bleomycin cardiotoxicity during chemotherapy for an ovarian germ cell tumor, Hippokratia 17 (2) (2013) 187–188.
[156] A. Skardal, S.V. Murphy, M. Devarasetty, I. Mead, H.-W. Kang, Y.-J. Seol, Y. S. Zhang, S.-R. Shin, L. Zhao, J. Aleman, A.R. Hall, T.D. Shupe, A. Kleensang, M. R. Dokmeci, S.J. Lee, J.D. Jackson, J.J. Yoo, T. Hartung, A. Khademhosseini, S. Soker, C.E. Bishop, A. Atala, Multi-tissue interactions in an integrated three-tissue organ-on-a-chip platform, Sci. Rep. 7 (2017).
[157] A.C. Daly, M.E. Prendergast, A.J. Hughes, J.A. Burdick, Bioprinting for the biologist, cell 184 (1) (2021) 18–32.
[158] L. Xu, S.R. Gutbrod, A.P. Bonifas, Y. Su, M.S. Sulkin, N. Lu, H.-J. Chung, K.-I. Jang, Z. Liu, M. Ying, C. Lu, R.C. Webb, J.-S. Kim, J.I. Laughner, H. Cheng, Y. Liu, A. Ameen, J.-W. Jeong, G.-T. Kim, Y. Huang, I.R. Efimov, J.A. Rogers, 3D multifunctional integumentary membranes for spatiotemporal cardiac measurements and stimulation across the entire epicardium, Nat. Commun. 5 (2014).
[159] D.T. Paik, M. Chandy, J.C. Wu, Patient and disease-specific induced pluripotent stem cells for discovery of personalized cardiovascular drugs and therapeutics, Pharmacol. Rev. 72 (1) (2020) 320–342.
[160] C. Sacchetto, L. Vitiello, L.J. de Windt, A. Rampazzo, M. Calore, Modeling cardiovascular diseases with hiPSC-derived cardiomyocytes in 2D and 3D cultures, Int. J. Mol. Sci. 21 (9) (2020).
[161] N. Huebsch, B. Charrez, G. Neiman, B. Siemons, S.C. Boggess, S. Wall, V. Charwat, K.H. Jaeger, D. Cleres, A. Telle, F.T. Lee-Montiel, N.C. Jeffreys, N. Deveshwar, A. G. Edwards, J. Serrano, M. Snuderl, A. Stahl, A. Tveito, E.W. Miller, K.E. Healy, Metabolically driven maturation of human-induced-pluripotent-stem-cell-derived cardiac microtissues on microfluidic chips, Nat. Biomed. Eng. 6 (4) (2022) 372–388.
[162] E. Karbassi, A. Fenix, S. Marchiano, N. Muraoka, K. Nakamura, X. Yang, C. E. Murry, Cardiomyocyte maturation: advances in knowledge and implications for regenerative medicine, Nat. Rev. Cardiol. 17 (6) (2020) 341–359.
[163] A. Acun, N. Trung Dung, P. Zorlutuna, In vitro aged, hiPSC-origin engineered heart tissue models with age-dependent functional deterioration to study myocardial infarction, Acta Biomater. 94 (2019) 372–391.